Published in : Sci. Immunol (2026), vol. 11, n°115
DOI: 10.1126/sciimmunol.ady7328
Status : Postprint (Author's version)

Cross-species cellular mapping and humanization of Fcγ receptors to advance antibody modeling

Karel F. A. Van Damme[1,2]*†, Dorine Sichien[1,2,3]†, Katrien Van der Borght[1,2,4,5]†, Justine Van Moorleghem[1,2], Sofie Van Gassen[6,7], Joseph Jorssen[8], Seppe De Winter[9,10], Elisabeth De Leeuw[1,2], Caihong Wang[11], Qingqing Chai[11], Anna Brotcke Zumsteg[11], Michael A. Schmid[11], Victor Bosteels[1,2,12], Pieter De Bleser[5,7], Manon Vanheerswynghels[1,2], Sofie De Prijck[1,2], Anna Bujko[5,13,14], Clint De Nolf[2,12,15], Martijn J. Schuijs[1,2,16], Bram Van Den Eeckhout[3], Ilse Rogiers[3], Robin Browaeys[6,17], Flore Thielemans[3], Katrien Quintelier[6,7,18], Jinke D'Hont[19,20], Tino Hochepied[19,20], Patricia Isnard Petit[21], Séverine Augier[22], Rachel Courtois[22], Stijn Verwaerde[1,2], Stijn Vanhee[1,2,23], Sjoerd Schetters[1,2], Charlotte L. Scott[5,13], Stein Aerts[9,10], Yvan Saeys[6,7], Alan J. Korman[11,24], Fabio Benigni[11], Davide Corti[11], Sophie Janssens[2,12], Niels Vandamme[5,25], Antonio P. Baptista[1,2], Christophe Desmet[8], Dirk Elewaut[2,26], Hamida Hammad[1,2], Ariane Morel[22], Eric Vivier[22,27,28], Fabiane Sônego[21], Kader Thiam[21], Sofie Voet[3], Bianca Balbino[3], Bart N. Lambrecht[1,2,18,29]*

[1]*Laboratory of Mucosal Immunology, VIB-UGent Center for Inflammation Research, Ghent University, Ghent, Belgium.*
[2]*Department of Internal Medicine and Pediatrics, Faculty of Medicine and Health Sciences, Ghent University, Ghent, Belgium.*
[3]*argenx, Ghent, Belgium.*
[4]*VIB Flow Core, VIB Center for Inflammation Research, Ghent, Belgium.*
[5]*Department of Biomedical Molecular Biology, Faculty of Sciences, Ghent University, Ghent, Belgium.*
[6]*Department of Applied Mathematics, Computer Science and Statistics, Ghent University, Ghent, Belgium.*
[7]*Data Mining and Modeling for Biomedicine Group, VIB-UGent Center for Inflammation Research, Ghent University, Ghent, Belgium.*
[8]*Laboratory of Cellular and Molecular Immunology, GIGA Institute, Faculty of Veterinary Medicine, University of Liège, Liège, Belgium.*
[9]*VIB Center for Brain & Disease Research, Leuven, Belgium.*
[10]*Department of Human Genetics, KU Leuven, Leuven, Belgium.*
[11]*Vir Biotechnology, San Francisco, CA, USA, and Bellinzona, Switzerland.*
[12]*Laboratory for ER Stress and Inflammation, VIB-UGent Center for Inflammation Research, Ghent, Belgium.*
[13]*Laboratory of Myeloid Cell Biology in Tissue Damage and Inflammation, VIB-UGent Center for Inflammation Research, Ghent, Belgium.*
[14]*Tribune Therapeutics, Oslo, Norway.*
[15]*Barriers in Inflammation, VIB-UGent Center for Inflammation Research, Ghent, Belgium.*
[16]*Cancer Research Institute Ghent, Ghent University, Ghent, Belgium.*
[17]*Bioinformatics Expertise Unit, VIB Center for Inflammation Research, Ghent, Belgium.*
[18]*Department of Pulmonary Medicine, Erasmus MC, Rotterdam, Netherlands.*
[19]*Transgenic Core Facility, VIB Center for Inflammation Research, Ghent, Belgium.*
[20]*Transgenic Core Facility, Department of Biomedical Molecular Biology, Ghent University, Ghent, Belgium.*
[21]*Genoway, Lyon, France.*
[22]*Innate Pharma, Marseille, France.*
[23]*Department of Head and Skin, Faculty of Medicine and Health Sciences, Ghent University, Ghent, Belgium.*

Published in : Sci. Immunol (2026), vol. 11, n°115
DOI: 10.1126/sciimmunol.ady7328
Status : Postprint (Author's version)

[24]*Bluesphere Bio, Pittsburgh, PA, USA.*
[25]*VIB Single Cell Core, Belgium.*
[26]*Molecular Immunology and Inflammation Unit, VIB Center for Inflammation Research, Ghent, Belgium.*
[27]*Aix Marseille Université, Centre National de la Recherche Scientifique, INSERM, Centre d'Immunologie de Marseille-Luminy, Marseille, France.*
[28]*Assistance Publique - Hôpitaux de Marseille, Hôpital de la Timone, Marseille Immunopôle, Marseille, France.*
[29]*Department of Respiratory Medicine, Ghent University Hospital, Ghent, Belgium.*
**Corresponding author. Email: karel.vandamme@ugent.be (K.F.A.V.D.); bart.lambrecht@ugent.be (B.N.L.)*
†These authors contributed equally to this work.

Abstract

Fc receptors mediate antibody effector functions. Immunoglobulin G (IgG), the predominant antibody in circulation and in clinical use, engages diverse Fc gamma (Fcγ) receptors differentially expressed across cell types. Here, we provide a comprehensive overview of Fcγ receptor and neonatal Fc receptor (FcRn) expression in humans, macaques, and mice. This analysis revealed substantial differences in Fcγ receptor diversity, cell-s pecific expression, and regulatory mechanisms that compromise the translation of mouse and macaque models for antibody research. To improve preclinical modeling, we generated a mouse in which humanized Fcγ receptors (FcγRI/CD64, FcγRIIA/CD32A, FcγRIIB/CD32B, FcγRIIIA/CD16A, and FcγRIIIB/CD16B), expressed under control of human promotors, replace their murine counterparts. This model also incorporates human FcRn to improve antibody pharmacokinetics. Humanization resulted in more faithful Fcγ receptor expression. We validated receptor functionality and demonstrated how cytokines modulate their expression. Together, this cross- species Fcγ receptor atlas and humanized mouse model can improve the preclinical evaluation of antibody-based therapeutics.

INTRODUCTION

Antigen recognition by antibodies induces effector functions such as target neutralization, complement activation, and cellular responses (1–3). More specifically, antibodies engage membrane-bound Fc receptors on various immune and nonimmune cells through interactions with their crystallizable (Fc) domain, leading to cytotoxicity, phagocytosis, antigen presentation, degranulation, release of inflammatory mediators, and cellular maturation (4).

Immunoglobulin G (IgG) is the most abundant antibody class in circulation and has been used extensively as the format for therapeutic antibodies. It interacts with different Fc gamma (Fcγ) receptors that exhibit remarkable diversity both within and between species (5, 6). In humans, IgG-activating Fcγ receptors include FcγRI (CD64), FcγRIIA (CD32A), FcγRIIC (CD32C), FcγRIIIA (CD16A), and FcγRIIIB (CD16B) (3, 7). In mice, IgG activates cells via FcγRI, FcγRIII (CD16), and FcγRIV (CD16.2), whereas macaque IgG activates cells through engagement of FcγRI, FcγRIIA, and FcγRIII. Shared across species, FcγRIIB (CD32B) is the only inhibitory Fcγ receptor capable of suppressing cellular responses. The neonatal Fc receptor (FcRn) enables transport across tissue compartments and mediates recycling of endocytosed IgG, explaining its long half-life (8). Differential affinities of four IgG subclasses (IgG1-4) for distinct Fcγ receptors (7, 9), their posttranslational modifications (4), and the presence of nonclassical Fcγ receptors such as CD209/DC- SIGN (10), CD23/FCER2 (11), Fc receptor like (12), and

Published in : Sci. Immunol (2026), vol. 11, n°115
DOI: 10.1126/sciimmunol.ady7328
Status : Postprint (Author's version)

TRIM21 (13) further add to the complexity of IgG-mediated responses. After Fcγ receptor engagement to monomeric immunoglobulins or multimeric immune complexes (ICs), signal transduction is initiated through recruitment of multiple intracellular proteins to immunoreceptor tyrosine- based activation (ITAM) or inhibition motifs in Fcγ receptors or adaptor proteins (FCER1G/FcRγ and CD247/CD3ζ) (10). The key role of these interactions is underscored by the presence of several Fcγ receptor polymorphisms that modulate the susceptibility to infectious and inflammatory disorders and determine the outcomes of IgG-mediated therapeutic interventions (6, 10, 14–18).

In drug design, the antibody Fc fragment sequence (4, 19) and/or glycosylation pattern (20) can be modified to improve half- life or alter effector functions. To comprehensively assess the impact of such modifications on pharmacokinetics and therapeutic efficacy, in vivo preclinical screening is essential. Traditionally, such screenings are conducted in mice and/or macaques. Disparities in Fcγ receptor genetics, binding affinities, and expression patterns, however, greatly limit the translatability of such studies to humans. To overcome these limitations, humanized mouse strains encoding human Fcγ receptors have been developed (21–26) and have greatly advanced our understanding of human antibody responses and the development of therapeutics (25, 27–29). Despite their value, these models suffer from limited availability, immaturity of the engrafted human immune system (25), and technical drawbacks related to their generation, such as transgene positional effects, altered endogenous gene regulation, and supraphysiological gene copy numbers (30). These issues also complicate mouse breeding and make it especially challenging to humanize specific epitopes.

Our present study aims to disentangle the diversity of Fcγ receptor expression between species. We map Fcγ receptors, including FcRn, across cell types at both mRNA and protein levels in humans, cynomolgus macaques, and mice. We evaluate which cytokines modulate their expression, and we predict transcription factors (TFs) that may control this dynamic regulation. To advance preclinical modeling, we developed a mouse model expressing the major humanized IgG–binding receptors on a murine Fcγ receptor–deficient background. We mapped the expression of the knockin humanized Fcγ receptors and FcRn among diverse cell populations and organs and evaluated their functionality across a range of antibody-dependent effector functions. Our Fcγ receptor resource and well- characterized humanized mouse model have the potential to advance research in human IgG biology and to enhance the preclinical evaluation of newly developed IgG- based immune interventions.

RESULTS

Comprehensive mapping of human Fcγ receptor expression and dynamics

Engagement of Fcγ receptors critically affects the efficacy and safety of IgG- based therapies. However, several recent evolutionary rearrangements in the low-/ intermediate- affinity Fcγ receptor gene locus generated diversity in human Fcγ receptors that is not present in rodents such as mice or even in primates such as macaques (Fig. 1) (31). Briefly, insertion of a noncanonical ITAM in FcγRIIA and a nonallelic homologous recombination event between FcγRIIA and FcγRIIB gave rise to the compound receptor FcγRIIC and to the duplication of FcγRIII in humans (31). Consistent with these genetic

Published in : Sci. Immunol (2026), vol. 11, n°115
DOI: 10.1126/sciimmunol.ady7328
Status : Postprint (Author's version)

rearrangements, alignment of Fcγ receptor protein sequences revealed large differences between species (fig. S1A).

Expression of human Fcγ receptors has been characterized previously (7, 22, 32, 33). Recent progress in the cellular annotation brought about by high- dimensional analysis of cells at the single- cell level prompted us to reassess Fcγ receptor expression in this refined immune landscape. Using 23-color spectral flow cytometry and single- cell sequencing, we defined Fcγ receptor expression in whole blood and in tissues of healthy individuals. By flow cytometry, FcγRI was detected on $CD14^{++}CD16^{-}$ classical monocytes and at minor levels on $CD14^{-}CD16^{++}$ nonclassical monocytes and $CD1c^{+}$ type 2 conventional dendritic cells (cDC2s) (Fig. 2A; fig. S1, B to D; and data file S1). FcγRIIA expression was high on neutrophils, eosinophils, monocytes, and cDCs; moderate FcγRIIA expression was found on basophils and platelets (Fig. 2B and fig. S1, E and F). FcγRIIB and FcγRIIC share an identical extracellular domain, being indistinguishable on flow cytometry staining. In most humans, however, FcγRIIC is not expressed because of premature stop codons (34). FcγRIIB/C was expressed by basophils and B cells; variable levels were noted on the monocytes and cDCs of the individuals examined, consistent with genetic and environmental variation in Fcγ receptor expression.

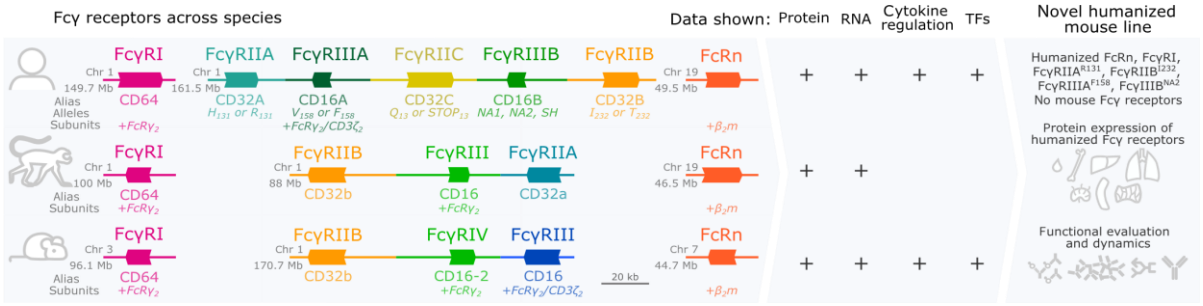

Fig. 1. Fcγ receptors across species, their genomic mapping, and the characterization of a mouse model with humanized Fcγ receptors. the genomic organization of the Fc receptor locus in human, cynomolgus macaque (*M. fascicularis*), and mouse is shown according to the ucSc genome Browser. Similar colors indicate genes that were predicted to be orthologs, and arrows indicate the orientation of the genes. heat-s hock proteins in the Fc receptor locus are not shown. in this resource, we mapped receptors at the protein and transcriptomic level and summarized the influence of cytokines and tFs on their expression. to bridge differences between species, we generated and characterized a mouse model carrying the major igg-b inding receptors.

Published in : Sci. Immunol (2026), vol. 11, n°115
DOI: 10.1126/sciimmunol.ady7328
Status : Postprint (Author's version)

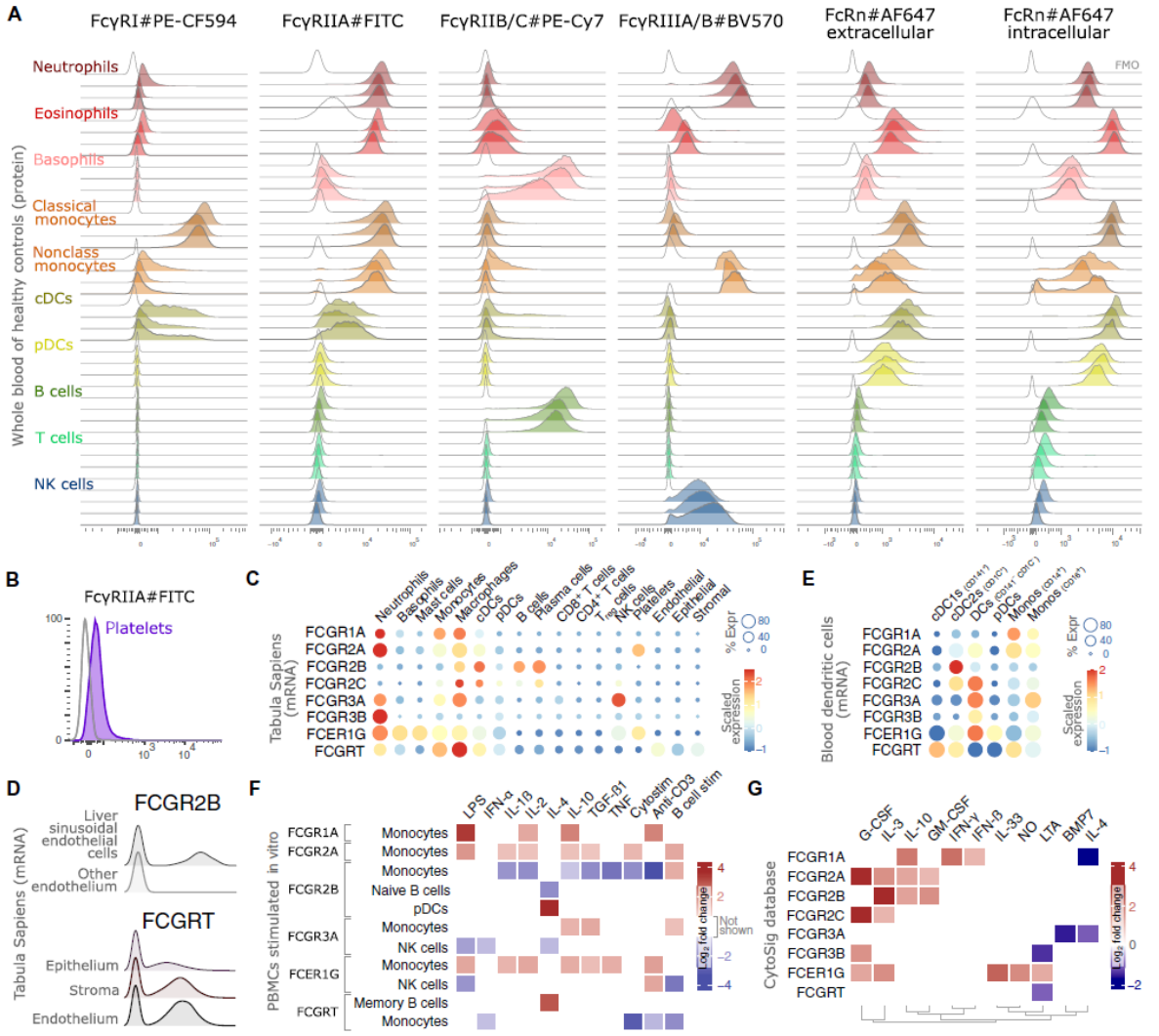

Fig. 2. Overview of human Fcγ receptors on cells in circulation and across organs and changes in expression levels during perturbations. (**A**) Protein expression of Fcγ receptors across cell populations, determined by flow cytometry in whole blood of healthy individuals. the gray, uncolored lines represent FMO controls (due to absence of CD16 in unstained control samples, $CD14^+$ monocyte population is also used as Fmo population for nonclassical monocytes). each filled line represents a biological replicate, data are representative for three independent experiments ($n = 3$ or 6 per experiment). (**B**) FcγRiia expression on platelets as determined by flow cytometry. (**C**) Single- cell mRna Fcγ receptor expression across cell types in the tabula Sapiens (*39*). t_{reg} cells, regulatory T cells. (**D**) *FcγRIIB* and *FCGRT* (FcRn) scaled transcript levels in nonimmune populations of the tabula Sapiens. (**E**) Fcγ receptor mRna expression of sorted circulating Dcs (*42*). Monos, monocytes. (**F**) Alterations in Fcγ receptor expression in cultured PBMCs after in vitro stimulation from (*48*). Only results with an absolute $\log_2$ fold change of greater than 1 and $P_{adj} < 0.05$ are shown. lPS, lipopolysaccharide; TNF, tumor necrosis factor. (**G**) Cytokines that affect Fcγ receptor transcript expression, based on the CytoSig database (*49*). For comparative visualization, histograms were normalized to their respective modes.

FcγRIIIA or its paralog FcγRIIIB lacking an inherent signaling domain was highly expressed by neutrophils, nonclassical monocytes, and $CD56^{dim}$ natural killer (NK) cells. FcRn, which can mainly be found intracellularly in the endosomes, was highly expressed in neutrophils, eosinophils, monocytes, and dendritic cells (DCs).

To better understand Fcγ receptor induction during hematopoiesis, we took advantage of a high-d imensional proteomic assay on human bone marrow (BM) cells (35, 36). After the identification of all major lineages and their precursors, we mapped the surface expression of Fc receptors across developmental stages (fig. S1, G and H). This analysis revealed that FcγRIIA/B/C (CD32) was up-r

Published in : Sci. Immunol (2026), vol. 11, n°115
DOI: 10.1126/sciimmunol.ady7328
Status : Postprint (Author's version)

egulated in both maturing eosinophils and neutrophils. In contrast, surface FcγRIIIA/B (CD16) expression was absent in early neutrophil progenitors but already present in early basophil and mast cell progenitors, highlighting a lineage-s pecific difference in Fc receptor induction. This observation is consistent with the reduction of mature $CD16^{+}$ neutrophils during sepsis, a condition characterized by emergency myelopoiesis and release of immature granulocytes (37, 38). Thus, the differential timing of Fc receptor expression across lineages may influence their levels and effector responses under altered BM output.

To expand this Fcγ receptor resource beyond the immune populations found in blood, we queried single- cell RNA sequencing (scRNA- seq) data from the Tabula Sapiens (39). The datasets in the Tabula Sapiens contain stromal, endothelial, epithelial, and immune cells from multiple tissues and donors. After exclusion of undetermined cells, erythrocytes, and progenitor cells, we mapped human Fcγ receptor transcripts (Fig. 2, C and D, and fig. S2, A and B). Among the immune cells absent in circulation, mast cells expressed *FCGRIIA* and macrophages transcribed all classical Fcγ receptors, except *FCGRIIIB*. Liver sinusoidal endothelial cells (LSECs) have been suggested to scavenge ICs through FcγRIIB (40); consistently, a substantial proportion of them demonstrated mRNA expression of this receptor (Fig. 2D). In line with proteomic data, *FCGRT* (encoding FcRn) was present in all myeloid cells. Variable amounts of *FCGRT* transcripts were found in all other cell types, including on a substantial proportion of endothelial, epithelial, and stromal cells (Fig. 2D and fig. S2C). *FCER1G*, which encodes the Fc receptor gamma chain (FcRγ or FcεR1γ) involved in signaling transduction downstream of FcεR1, FcαR, FcγRI, and FcγRIIIA in humans (3, 41), was actively transcribed by all cells engaged in activating Fcγ receptor signaling (fig. S2B). In line with protein data, *FCGR2A* transcripts could be detected in platelets, as could *FCER1G* transcripts. Given that antigen-p resenting cells were underrepresented and poorly annotated in the Tabula Sapiens, we further studied single- cell data from DCs sorted from blood (Fig. 2E) (42). This analysis indicated more transcription of *FCGRIIA* and *FCGRIIB* in $CD1C^{+}$ cDC2s in comparison with $CD141^{+}$ cDC1s and high levels of *FCGRT* across both DC subsets.

Aside from receptor expression on the cell surface, cellular responses upon IgG binding are likely to be influenced by the variety of kinases able to phosphorylate intracellular tails of the Fcγ receptors or their adaptor proteins (FcRγ or CD3ζ). As compiled in the decoupleR database (43), some kinases seemed to exhibit Fcγ receptor specificity, whereas others, such as BLK, FYN, LYN, SRC, and SYK, were promiscuous (fig. S2D).

Various inflammatory stimuli can modulate Fcγ receptor expression or signaling (44–47). To assess this systematically, we analyzed single- cell transcriptomics of peripheral blood mononuclear cells (PBMCs) exposed to 11 common stimuli in vitro from Wood *et al.* (48). All perturbations significantly altered Fc receptor transcription (Fig. 2F, fig. S2E, and data file S2). These effects were cell-type–specific; for example, lipopolysaccharide (LPS) reduced Fc receptor expression in NK cells while up- regulating *FCGR1A* and *FCGR2A* in monocytes. Several changes also reflected indirect regulation given that T cell– (anti-C D3 and CytoStim) and B cell–directed stimuli (human embryonic kidney 293 cells expressing CD40L and anti- CD79B) modified Fc receptor transcription in monocytes and NK cells.

To extend these observations and capture signaling events not represented in PBMCs, we turned to prior knowledge models. Using CytoSig (Fig. 2G and fig. S2F) (49) and NicheNet (fig. S2G) (50, 51), we

Published in : Sci. Immunol (2026), vol. 11, n°115
DOI: 10.1126/sciimmunol.ady7328
Status : Postprint (Author's version)

mined these datasets in a cell-t ype–agnostic manner. Both resources identified type I and II interferons (IFNs) and interleukin 10 (IL- 10) as major drivers of Fcγ receptor transcription. Common β- chain cytokines IL- 3 and granulocyte- macrophage colony- stimulating factor (GM-C SF) were also predicted to promote accumulation of *FCGRIIA* and *FCGRIIB* transcripts. In contrast, IL-4 suppressed Fcγ receptor expression, with the exception of *FCGRIIB* and *FCGRT*, in keeping with its established role as a repressor of Fcγ receptor signaling (fig. S2F) (52). Together, these results highlight the broad impact of inflammatory contexts on antibody responses.

To understand the gene networks regulating Fcγ receptor expression, we queried the NicheNet gene regulatory database (Fig. 3A) (50, 51) and evaluated these predictions using a gene regulatory network (GRN) inference on human PBMCs using SCENIC+ (53). SCENIC+ makes use of combined chromatin accessibility and gene expression and TF motifs to infer TFs and enhancers for target genes. This independent, data- driven analysis was able to recover several TFs in line with the large- scale data compiled in NicheNet, including ETS- TFs (ETS1, ELF2, and SPI1), signal transducers and activators of transcription (STATs), interferon regulatory factors, USF, and FOS (Fig. 3B, data file S3, and https://genome-euro.ucsc.edu/s/kfvdamme/Gene_Regulatory_Networks). To verify these predictions, we next analyzed perturbation experiments of Encode deeply profiled cell lines (*53*, *54*) (data file S4). We found that targeting of several of these predictions, including NFYA, USF1, GATA1/2, and STAT1/2/5A/6, resulted in loss of *FCGR2A* in the myeloid cell line K562 ($\log_2$ fold change < -2.5 for all TFs). To differentiate direct from indirect TF effects, we examined chromatin immunoprecipitation sequencing (ChIP-seq) peaks in the *FCGR2A* locus. We found binding of STAT5A, STAT2, and USF1, suggesting that these TFs may directly control transcription of *FCGR2A* (Fig. 3C). *FCGRT* was strongly down- regulated after perturbation of several TFs in the liver cell line HepG2, of which XRCC5 and ZC3H8 ($\log_2$ fold changes, -2.1 and -1.6, respectively) bind in genomic regions closely linked to *FCGRT* expression (Fig. 3D). Together, these integrated datasets illustrate the context-specific expression and regulation of human Fcγ receptors and highlight the need for a systems-level understanding of their biology when designing antibody- mediated interventions.

Human, murine, and macaque Fcγ receptors exhibit substantial biological differences

Mice and nonhuman primates are essential to model the effects of antibody- based drugs to try to predict how the molecules will behave in humans. To compare IgG-mediated responses in these models with those in humans, we aimed to map murine and macaque Fcγ receptor expression.

We delineated Fcγ receptor protein expression in C57BL/6J mice, given that these mice are the most commonly used model organisms for translational research. Both in blood and in tissues (Fig. 4A and data files S5 and S6), mouse FcγRI (mFcγRI) expression was found only on macrophages, which contrasted with humans in which FcγRI expression was broader. mFcγRIIB expression by eosinophils, basophils, mast cells, macrophages, B cells, and a small subset of NK cells was similar to human FcγRIIB, with notable exceptions of this receptor being also detected on monocytes and cDC1s in mice. In the heterogeneous splenic cDC2 compartment, endothelial cell– selective adhesion molecule–negative ($Esam^-$) cDC2Bs expressed FcγRIIB in contrast with $Esam^+$ cDC2As (Fig. 4B) (55–57). Liver endothelial cells (ECs) expressed high levels of mFcγRIIB involved in regulating the half-l ife of circulating ICs (58),

Published in : Sci. Immunol (2026), vol. 11, n°115
DOI: 10.1126/sciimmunol.ady7328
Status : Postprint (Author's version)

with slightly higher expression on LSECs as compared with that on non- LSECs and no spatial effect of zonation along the portal- central axis (Fig. 4C).

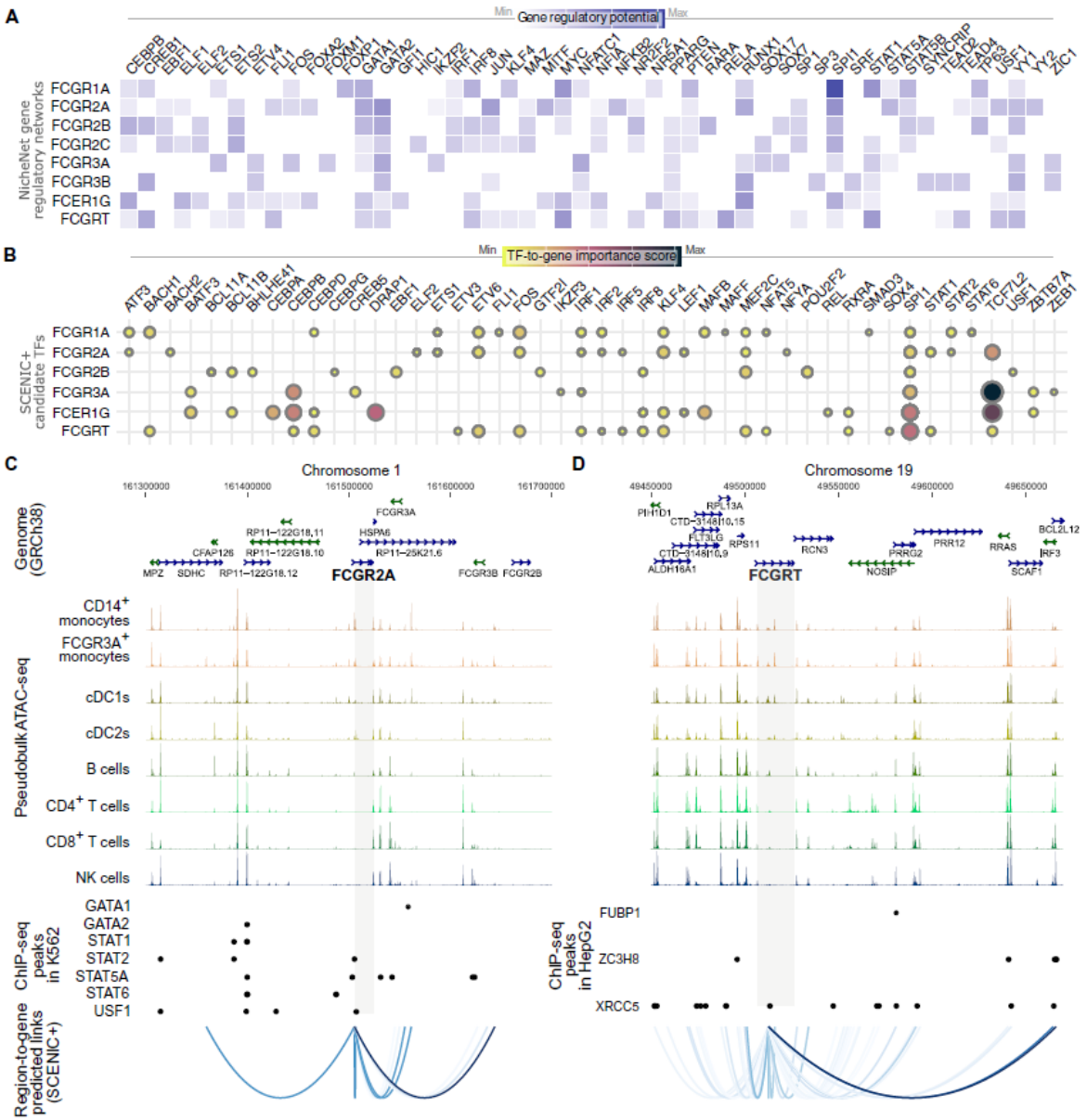

Fig. 3. Integrative analysis of GRN controlling human Fcγ receptor and FcRn expression. (**A** and **B**) TFs regulating Fcγ receptor transcription, showing predicted gene regulatory potential scores from nichenet (*50, 51*) (a) and TF- to- gene importance score inferred by SCENIC+ (*53*) applied to human PBMCs (B). Color scales indicate higher scores. (**C** and **D**) Genomic loci of *FCGR2A* (c) and *FCGRT* (D). Tracks display lineage- specific chromatin accessibility in human PBMCs (pseudobulk ATAC-seq from 10X Multiome). ChIP-seq binding peaks from cell lines for TFs identified in perturbation experiments. Arcs highlight genomic accessibility correlated with gene expression as inferred by SCENIC+, with stronger links in darker colors.

Published in : Sci. Immunol (2026), vol. 11, n°115
DOI: 10.1126/sciimmunol.ady7328
Status : Postprint (Author's version)

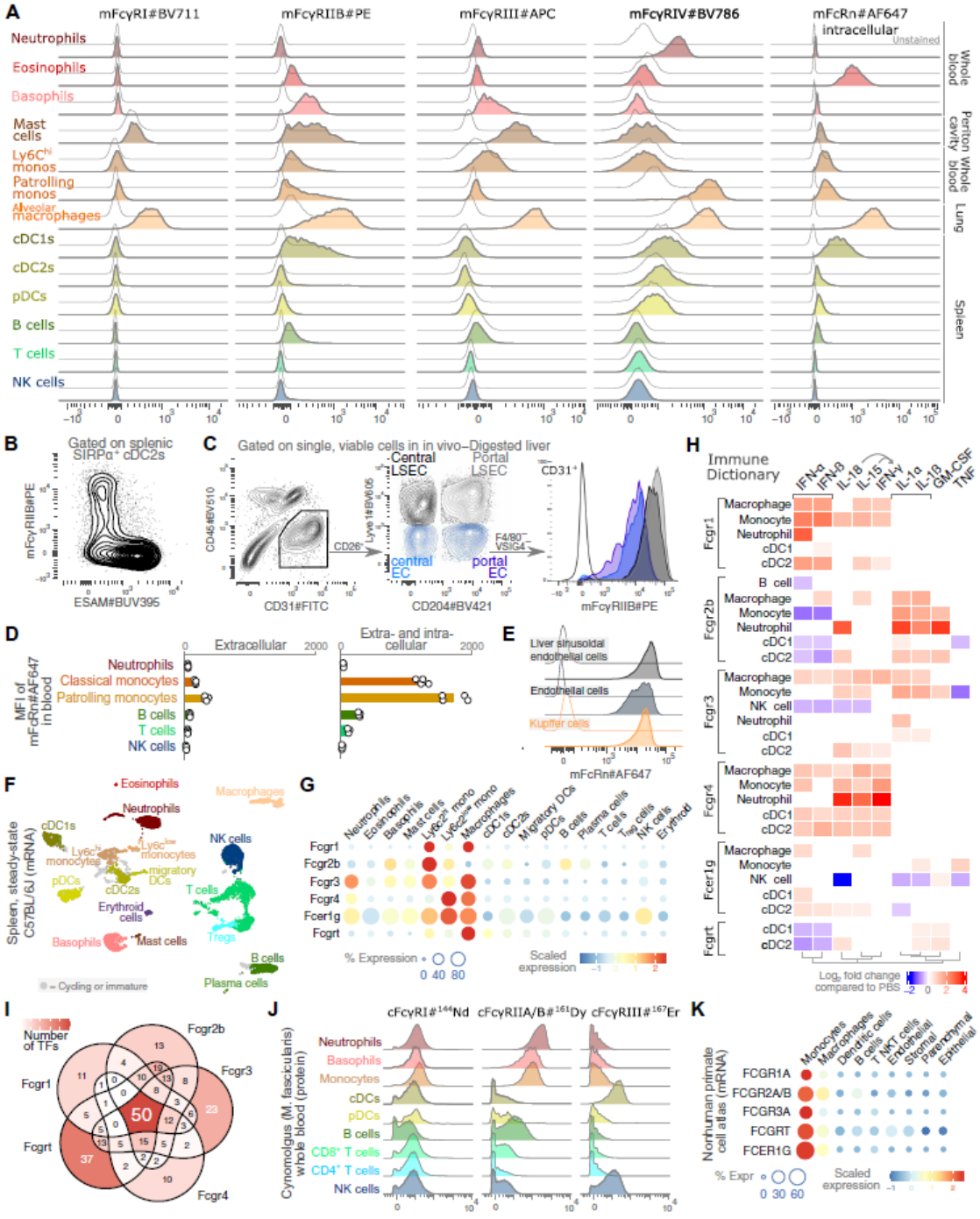

Fig. 4. Murine and macaque Fcγ receptor expression and their alterations during inflammation. (**A**) Murine expression of Fcγ receptors at the cell surface and intracellular FcRn. Data are representative for three independent experiments ($n = 4$ per experiment). Uncolored lines represent unstained controls. Periton cavity, peritoneal cavity. (**B**) ESAM and FcγRIIB expression on splenic SIRPα$^+$ cDc2s. (**C**) gating of endothelial and sinusoidal cells in the liver (*75*) and their FcγRiiB expression. (**D**) Mouse FcRn expression at the cell surface or intracellularly, as determined in whole blood using flow cytometry. (**E**) intracellular FcRn levels in murine liver cells. (**F**) UMAP of scRNA-seq on sorted splenocytes of C57Bl/6J mice. (**G**) Fcγ receptor transcript levels in the spleen. (**H**) Cytokines upstream of murine Fcγ receptor transcription in lymph nodes, according to the immune Dictionary (*63*). (**I**) Venn diagram highlighting unique and shared TFs with a regulatory potential of >1 across mouse Fcγ receptors. (**J**) Surface staining of Fcγ receptors in whole blood from *M. fascicularis*, measured using CyTOF (*69*). (**K**) Cynomolgus monkey Fcγ receptor transcript levels from the nonhuman primate transcriptomic atlas (*70*). all histograms were normalized to their respective maximal frequencies.

Published in : Sci. Immunol (2026), vol. 11, n°115
DOI: 10.1126/sciimmunol.ady7328
Status : Postprint (Author's version)

mFcγRIII expression differed from the human FcγRIIA expression profile in the absence of detection on DCs and NK cells, whereas it was detected on granulocytes, mast cells, and macrophages. mFcγRIV was expressed by neutrophils, patrolling monocytes, and macrophages. Fcγ receptor expression varied considerably between organs, e.g., cDC2s in lymphoid tissues had barely detectable Fcγ receptors, whereas lung cDC2s demonstrated high expression of mFcγRIIB (fig. S3A). This tissue- specific expression pattern may reflect a shift in cDC2 subsets, which have been defined by their Fcγ receptor expression profile (56, 59). Compared with intracellular staining, mFcRn was detected poorly on the cell surface (Fig. 4D). Intracellularly, we observed lower levels of FcRn on murine neutrophils and basophils compared with their human counterparts (Fig. 4A), whereas eosinophils exhibited unexpectedly high FcRn levels in both species. Nonimmune cells also contribute to IgG and albumin turnover through FcRn (60, 61), and, accordingly, LSECs and other liver ECs exhibited high FcRn expression (Fig. 4E).

To map mouse Fcγ receptors at a transcriptomic level, we next examined RNA-s eq data from the Tabula Muris (62). Our analysis focused on fluorescence- activated cell sorting (FACS)–captured cells after removal of stem and progenitor cells and organs from which no immune cells were sequenced. Among structural cells, *Fcgrt* expression was particularly pronounced in stromal cells and ECs, consistent with human data (fig. S3B). Because only a limited number of immune cell types were represented in the Tabula Muris, we carried out a scRNA- seq experiment on splenocytes from female C57BL/6J mice. Through a combination of cellular sorting and a microwell capture system, we enriched for nonabundant and fragile populations that are, otherwise, absent in single- cell datasets, identifying diverse rare immune subsets, including splenic basophils, mast cells, and eosinophils (Fig. 4F, fig. S3C, and data file S7; see portal: www.single-c ell.be/splenic_immune_cell_compartment). In steady state, *Fcgr1* was transcribed by macrophages and *Ly6c2*^{hi} monocytes (Fig. 4G). In contrast with human *FCGR1A*, mouse *Fcgr1* was not transcribed by neutrophils. *Fcgr2b* was transcribed by basophils, mast cells, monocytes, cDCs, B cells, and some NK cells, whereas murine splenic macrophages did not transcribe *Fcgr2b*, contrary to macrophages in the Tabula Sapiens (Fig. 2C). *Fcgr3* transcripts were detected in all granulocytes, monocytes, and macrophages and at low levels in NK cells. Consistent with our cytometry results, mouse cDCs did not express activating receptors. With the exception of NK cells, the human *FCGR3A* expression profile aligned well with murine *Fcgr4* transcription, which was detected on neutrophils, monocytes, and macrophages. As in humans, *Fcer1g* (FcRγ), which is required for signal transduction of all activating Fcγ receptors in mice, was expressed by myeloid cells and NK cells. Except for neutrophils, the *Fcgrt* expression pattern aligned well between humans and mice.

Fc receptors influence and are influenced by inflammation (45, 46). To gain insights into the latter topic, using the Immune Dictionary data (63), we mapped the changes in murine Fcγ receptor transcription in lymph nodes 4 hours after stimulation with cytokines (Fig. 4H and fig. S3D). Overall, most murine Fcγ receptors seemed to have their expression regulated by similar cytokines modulating human expression, namely, type I and II IFNs, IL- 1α/β, and GM- CSF. Transcriptional regulation of *Fcgr4* mirrored that of Fcgr1. Unexpectedly, however, well- known NK cell stimulators such as IFNs, IL- 2, IL- 15, and IL-1 8 significantly decreased *Fcgr3* transcription (64). We could corroborate this unexpected effect of common γ chain cytokines on NK cell *FcγRIII* expression in an independent ImmGen dataset (fig. S3E) (65).

Published in : Sci. Immunol (2026), vol. 11, n°115
DOI: 10.1126/sciimmunol.ady7328
Status : Postprint (Author's version)

To further disentangle the dynamic and species-s pecific nature of Fcγ receptor expression, we compiled the TFs likely to influence mouse Fcγ receptor transcription. On the basis of large-s cale integrated ChIP- seq data (66), we scored the regulatory potential for each TF within 10 kb of each Fcγ receptor transcription start site (TSS) using an exponential decay function (data file S8) (67). This analysis revealed a number of cis–regulatory elements shared between all mouse Fcγ receptors (Fig. 4I). Alignment of TFs with the highest regulatory potential between humans and mice indicated an incomplete overlap (fig. S3, F and G). These findings suggest that lineage-determining factors and cell-cell communication events regulate the cellular Fcγ repertoire through a limited number of TFs, which are only partially conserved across species. Hence, the use of mice as an organism in which to model human IgG biology may be considered inadequate.

Our analysis suggests that, despite extensive ex and in vivo modeling, side effects of monoclonal antibodies may appear only during trials with human participants. To minimize this risk, nonhuman primates are regularly used in drug development and toxicology screening, given that they are thought to better reflect human physiology and share many targeted epitopes (68). Despite these advantages, cynomolgus and rhesus macaques (*Macaca fascicularis* and *Macaca mulatta*, respectively) do not display a similar diversity of human Fcγ receptors (Fig. 1) (*31*). To delineate protein expression of Fc receptors in cynomolgus macaques, we analyzed publicly available cytometry by time-o f- flight (CyTOF) data (Fig. 4J; fig. S4, A and B; and data file S9) (69). Whereas expression of cynomolgus FcγRII (cFcγRIIA) or cFcγRIIB, detected by the same antibody clone in neutrophils, basophils, monocytes, and B cells, paralleled that of human FcγRIIA and human FcγRIIB, scant expression of cFcγRIA in circulating cells contrasted with our observations in humans. Similarly, the absence of cFcγRIII in granulocytes conflicted with the human situation. Transcriptionally, we mined the single- nucleus and scRNA- seq nonhuman primate cell atlas (70) for Fcγ receptor expression (Fig. 4K and fig. S4C), confirming the protein data. Thus, despite the contributions of nonhuman primates to biomedical research, significant differences in Fcγ receptors complicate their use for preclinical antibody modeling.

A humanized mouse line with knockin humanized Fcγ receptors faithfully recapitulates human Fcγ receptor expression

To circumvent crucial interspecies differences in Fcγ receptor biology, we genetically modified mice to express humanized Fcγ receptors. On the basis of differential use of distinct TFs by humans and mice, we opted to knockin the Fcγ receptor coding sequences under the control of the relevant human regulatory landscape. Briefly, in two independent steps, we inserted humanized FcγRI (hFcγRI) and humanized FcγRIIA/IIB/IIIA/IIIB (hFcγRIIA/IIB/IIIA/IIIB) in the endogenous murine locus through homologous recombination. These cells were then used to create hFcγRI and hFcγRIIA/IIB/IIIA/IIIB knockin heterozygous mice, which were bred together to obtain homozygous hFcγR^{ki} mice, so called genO- hFcgR. The lower-a ffinity alleles FcγRIIA^{R131}, FcγRIIB^{I232}, FcγRIIIA^{F158}, and FcγRIIIB^{NA2} were chosen in line with a previously established Fcγ humanized mouse strain (21). FcγRIIC, which is nonfunctional in most of the human population (34), was not introduced. Humanized Fcγ receptor mice were interbred with a humanized FcRn line (71) to generate sextuple knockin hFcγR/hFcRn^{ki} animals, also called genO- hFcγR/hFcRn. Knockin Fcγ receptor expression was controlled by the human promotors,

Published in : Sci. Immunol (2026), vol. 11, n°115
DOI: 10.1126/sciimmunol.ady7328
Status : Postprint (Author's version)

whereas humanized FcRn remained under control of the mouse promotor. All constructs disrupted endogenous mouse Fcγ receptor including FcRn genes, preventing their expression.

hFcγR^{ki} and hFcγR/hFcRn^{ki} mice appeared healthy and had normal body weights (fig. S5A). hFcγR^{ki} mice produced offspring at normal Mendelian frequencies, whereas hFcγR/hFcRn^{ki} mice produced offspring with fewer female than male pups (40 and 60%, respectively). Concentrations of mouse IgA, IgE, and IgM were similar across genotypes, although IgG levels were strongly decreased in hFcγR/ hFcRn^{ki} mice because of impaired recycling of mouse IgG by humanized FcRn (fig. S5B) (72). Knockin mice did not display signs of inflammation or damage on histology (fig. S5C) and had equal numbers of immune cells as determined by flow cytometry across organs (fig. S5, D and E). Consistent with the genetic targeting, we confirmed the absence of mouse Fcγ receptors in hFcγR^{ki} mice (fig. S5F).

Next, we examined the expression of the humanized Fcγ receptors across various tissues (Fig. 5A and data file S10). Humanized FcγRI was expressed on the surfaces of monocytes and macrophages (except on splenic red pulp macrophages) (Fig. 5B). Neutrophils in circulation did not express hFcγRI, whereas they did at low levels in tissues (Fig. 5C and fig. S6A).

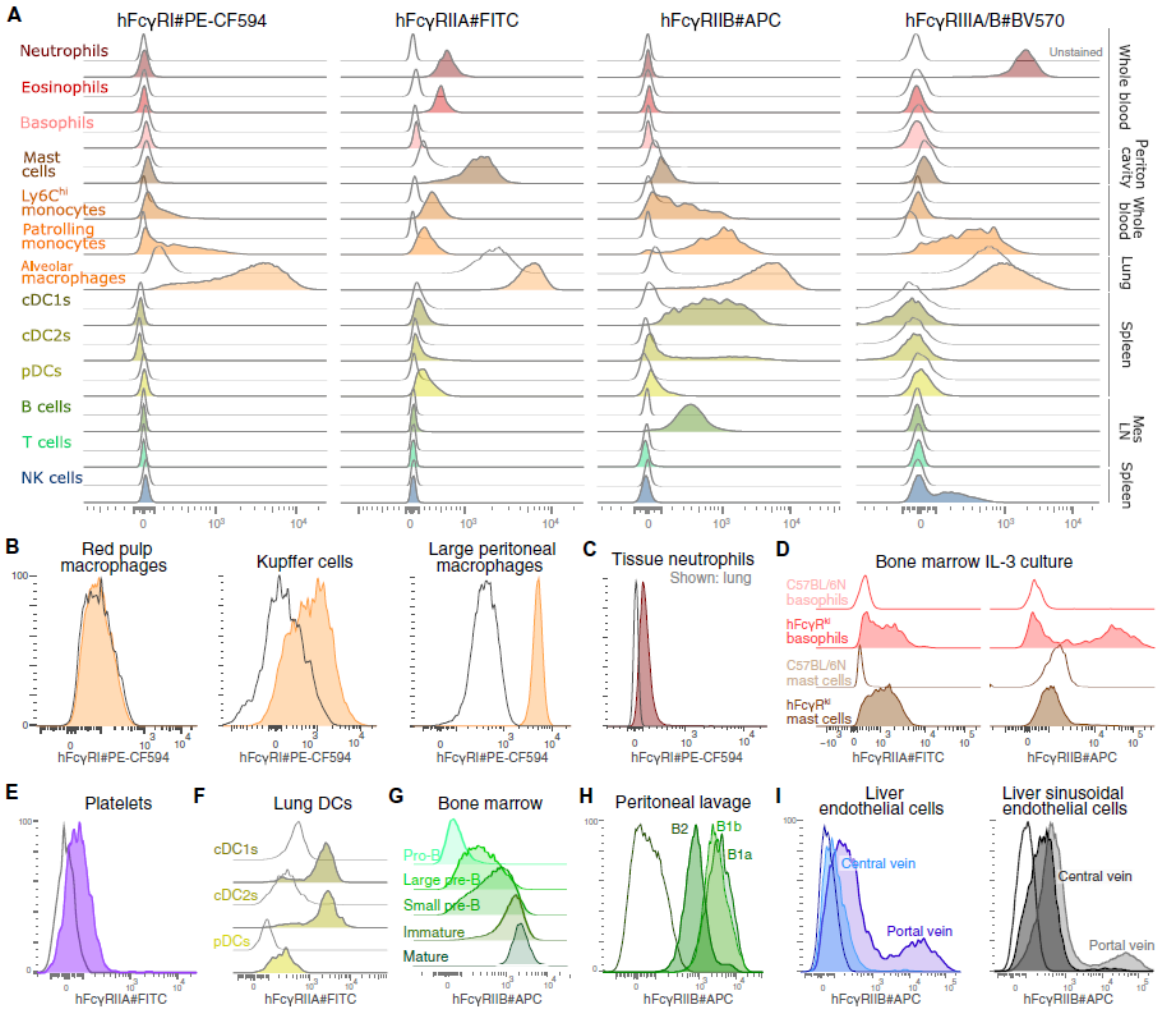

Fig. 5. The Fcγ receptor expression profile in a humanized mouse line. (**A**) Surface expression of hFcγ receptors across immune populations and organs in hFcγR^{ki} mice. Gray lines represent populations of pooled sample unstained for Fcγ receptors. MesLN, mesenteric lymph node. (**B** and **C**) Surface hFcγRi in macrophages (B) and neutrophils (c) across tissues. (**D**) Expression of hFcγRIIA or hFcγRIIB in basophils or mast cells from a BM-

Published in : Sci. Immunol (2026), vol. 11, n°115
DOI: 10.1126/sciimmunol.ady7328
Status : Postprint (Author's version)

derived culture supplemented with IL-3. (**E**) hFcγRIIA expression on hFcγR^{ki} platelets isolated from whole blood. (**F**) Lung Dc subset expression of hFcγRiia. (**G**) hFcγRiiB expression during B cell development in the BM. (**H**) B1 and B2 cell hFcγRiiB expression in the spleen. (**I**) Expression of hFcγRiiB on ECs and LSECs. All data are representative for two independent experiments ($n = 3$ per experiment). Uncolored lines represent unstained controls, unless marked otherwise, and histograms were scaled to normalize modal values.

hFcγRIIA expression was widespread among myeloid populations, with an exception being its absence from basophils. Although this observation was unlike the human situation, hFcγR^{ki} basophils could be induced to express hFcγRIIA and hFcγRIIB in vitro by stimulation with IL- 3 (Fig. 5D and fig. S6, B and C). As in humans, hFcγRIIA was expressed by platelets (Fig. 5E and fig. S6, D and E). Humanized Fcγ receptor expression varied across tissues (for instance, hFcγ receptor was higher on lung cDCs as compared with lymphoid tissue cDCs), suggesting that the inserted receptors remain sensitive to context-dependent modulation (Fig. 5F and fig. S6F). hFcγRIIB expression was found on monocytes, macrophages, cDC1s, and B cells. FcγRIIB represents a checkpoint in antibody- producing cells (73, 74). Consistently, its expression increased progressively during B cell development in the BM of hFcγR^{ki} mice (Fig. 5G), and it was higher on natural antibody- producing B1 cells, as compared with B2 cells in the peritoneal cavity (Fig. 5H and fig. S6G). A proportion of liver ECs expressed high levels of humanized FcγRIIB, particularly those present around portal zones of the liver (coexpressing CD204) (Fig. 5I and fig. S6H) (75). hFcγRIIIA/B was present on neutrophils, patrolling monocytes, macrophages, and 40% of NK cells in the spleen and lung (fig. S6, I and J).

Representative modeling of human IgG–mediated responses requires not only cognate Fcγ receptors but also physiological antibody levels, which are predominantly regulated by FcRn. However, human IgG has a 10- fold higher affinity for mouse FcRn compared with human FcRn, which affects the half-l ife of administered human IgGs (76). To address this issue, we examined our sextuple hFcγR/ hFcRn^{ki} mice and validated humanized FcRn expression in the spleen and peritoneal cavity (fig. S6, K and L). hFcRn expression, driven by its mouse promotor as previously described (71), was detected in monocytes, macrophages, mast cells, and DCs. Collectively, these data indicate that hFcγR/hFcRn^{ki} mice express all knockin humanized IgG receptors with a pattern that closely mirrors that of humans, without disturbing immune cell development.

The knockin humanized Fcγ receptors are functional

To evaluate the functionality of the knockin humanized Fcγ receptors, we designed a set of experiments to test the inducibility and effector functions of distinct Fcγ receptors on various cell types. Our earlier data underscored the highly dynamic regulation of Fcγ receptor expression in both humans and mice. To assess whether the knockin receptors in hFcγR/hFcRn^{ki} mice would be equally responsive to perturbations, we administrated 5 μg of different mouse cytokines (IFN- α, IFN- γ, GM-CSF, IL-4 , and IL-10) or phosphate- buffered saline (PBS) intravenously. Sixteen hours after this challenge, Fcγ receptor expression at the protein level was evaluated in splenocytes, revealing significant alterations for all humanized Fcγ receptors across several immune populations (data files S11 and 12). Consistent with expectations, hFcγRI was up- regulated in myeloid cells by type I and II IFN (Fig. 6A). hFcγRIIA expression on monocytes was enhanced by IFNs, GM- CSF, and IL- 10. Reflecting IL- 10's immunoregulatory role, hFcγRIIB was increased on B cells. hFcγRIIIA/B on monocytes increased in response to IFNs, whereas GM-C SF slightly decreased its expression on neutrophils. Additionally, intracellular hFcRn in myeloid cells increased upon IFN- γ stimulation. These results demonstrate that

Published in : Sci. Immunol (2026), vol. 11, n°115
DOI: 10.1126/sciimmunol.ady7328
Status : Postprint (Author's version)

the humanized promotors in the hFcγR/hFcRn^{ki} mice enable transcriptional reprogramming of Fc receptors in response to mouse cytokines in vivo.

To evaluate Fcγ receptor–dependent functions in vivo, we subjected hFcγR^{ki} mice to an influenza A model (77, 78). Two days before infection, monoclonal human antibodies with distinct Fcγ receptor binding properties were administered. Broadly neutralizing anti- hemagglutinin IgG1 antibodies in an Fc dead IgG1-G RLR format (G236R/L328R) (79) provided only minimal protection against a lethal viral challenge compared with wild-t ype human IgG1 (Fig. 6B and fig. S7A), demonstrating the critical importance of Fcγ receptor engagement in antiviral immunity. Fc engineering moreover enhanced antibody efficacy compared with wild-t ype IgG1 given that IgG1- GA (G236A) improved weight loss recovery because of its increased binding to FcγRIIA (80), whereas IgG1- GAALIE (G236A/ A330L/I332E) further improved outcomes through enhanced binding to FcγRIIA and FcγRIIIA/B and reduced affinity for FcγRIIB (81, 82). Enhanced protection by Fc optimized monoclonal antibodies was not due to altered pharmacokinetics given that antibody levels in serum were similar after dosing (fig. S7B). Collectively, these data validate the utility of hFcγR^{ki} for studying Fc-mediated effector function during viral infections and show the potential of this model to rank lead molecules according to efficacy.

We next assessed the functions of individual humanized Fcγ receptors. First, we focused on hFcγRI induction and expression by cDC2s upon sensing of type I IFNs, which is known to promote IgG- driven antigen uptake and presentation (46). To this end, we generated hFcγR^{ki} DCs from FLT3L BM cultures, which we stimulated with IFN- α and ovalbumin (OVA). OVA was delivered to the cell cultures either as a free antigen or as an IC formed with OVA- specific human IgG1 antibodies (Fig. 6C). For the latter, two recombinantly produced antibody clones were used, with either a wild- type or an Fc dead (LALAPG; L234A/L235A/P329G) backbone, targeting distinct OVA epitopes to allow multimerization as shown by size exclusion–high- performance liquid chromatography (SEC-H PLC) (Fig. 6D). Type 1 IFN stimulation led to a marked up-regulation of humanized FcγRI on cultured cDC2s, but not on cDC1s (Fig. 6E). After administration of OVA- IgG1 ICs, but not soluble OVA or Fc dead OVA-I Cs, hFcγRI on cDC2s was rapidly internalized from the cell surface, promoting enhanced OVA uptake (Fig. 6F and fig. S7, C and D). Internalization of OVA was confirmed by imaging cytometry (Fig. 6G). The increase in hFcγRI-d ependent antigen presentation was reflected in increased T cell proliferation and elevated IL-2 and IFN- γ secretion upon coculture of BM-derived cDC2s and OVA- specific OT- II CD4^{+} T cells (Fig. 6H). Together, our data demonstrate that knockin humanized receptors can boost antigen uptake and presentation.

We also generated monoclonal anti- CD20 antibodies (83) with diverse human or mouse Fc formats and assessed their effects on B cell depletion in circulation and tissues (Fig. 6I). In FcγR^{ki} mice, murine IgG2a achieved only modest B cell depletion compared with Fc competent human IgG1 given that mouse IgGs interact less with human FcγRIIA and FcγRIIIA (84). Monoclonal antibodies with enhanced FcγRIIIA receptor binding, such as afucosylated (85) or GASDALIE mutated (G236A/S239D/A330L/I332E) (*21*) antibodies, improved antibody-dependent cellular cytotoxicity (ADCC) (Fig. 6I). On the other hand, B cell depletion induced by IgG1 with LALAPG mutations was reduced, underscoring the value of these humanized mice for evaluating depleting efficacy.

To functionally evaluate effector mechanisms specifically downstream of hFcγRIIA, we used heat-aggregated human ICs. This serves as a model of passive systemic anaphylaxis that depends on

Published in : Sci. Immunol (2026), vol. 11, n°115
DOI: 10.1126/sciimmunol.ady7328
Status : Postprint (Author's version)

hFcγRIIA^{+} neutrophils and platelets (22, 24). Administration of 0.5 mg of heat- aggregated human immunoglobulins intravenously (IVIgs) induced a transient temperature drop in hFcγR^{ki} mice, but not in mice lacking FcRγ (FcεR1γ$^{-/-}$) (Fig. 6J). This indicates that engagement of humanized Fcγ receptors induces the release of inflammatory mediators.

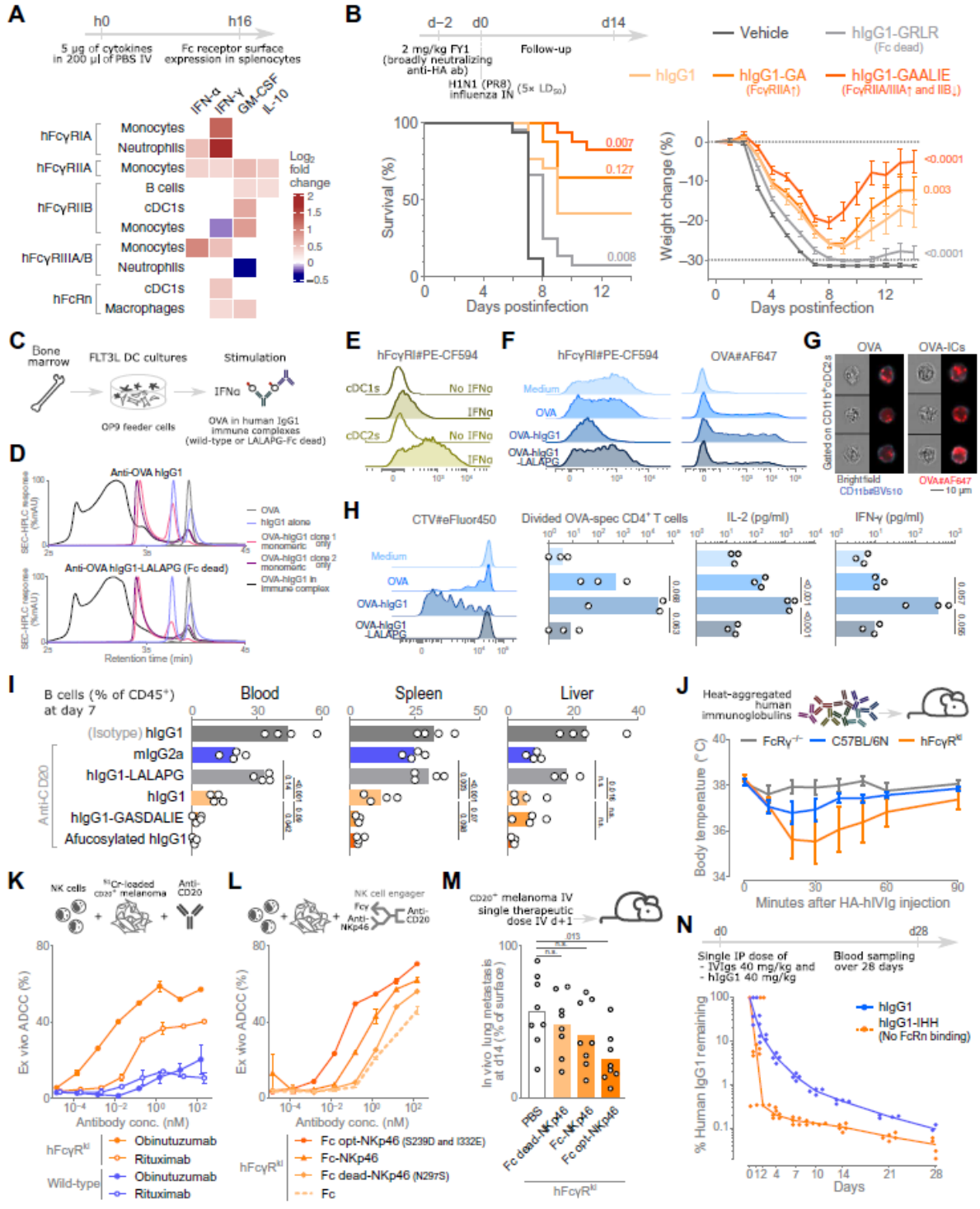

I

Published in : Sci. Immunol (2026), vol. 11, n°115
DOI: 10.1126/sciimmunol.ady7328
Status : Postprint (Author's version)

Fig. 6. Effector mechanisms mediated by knockin humanized Fcγ receptors. (**A**) Receptor dynamics after cytokine administration in hFcγR/hFcRn^{ki} mice, expressed as log_2 fold changes. expression of the humanized receptors was assessed on splenocytes 16 hours (h) after cytokine stimulation. only results where the false discovery rate was < 0.05 are shown. IV, intravenous. (**B**) Human antibody–mediated protection against an influenza infection in hFcγR^{ki} mice, shown as survival (left) or weight curves (right). Mice received Fy1 (2 mg/kg), a broadly neutralizing anti- hemagglutinin antibody, in distinct Fc formats intravenously 2 days (d) before a challenge with 5× LD_{50} of A/Puerto Rico/8/34 (PR8) H1N1 virus. (**C**) Schematic of BM-derived DC assay. (**D**) SEC- HPLC of combinations of OVA and OVA-specific human IgG1 antibodies in wild-t ype or Fc dead format (top and bottom, respectively). (**E**) Induction of humanized FcγRi in BM-derived DCs stimulated with iFN- α. (**F**) Representative example of surface expression of hFcγRi and OVA uptake by cDC2s from hFcγR^{ki} Bm, after stimulation with iFN- α and medium, OVA, or OVA in ics. (**G**) AF647- labeled OVA uptake by cDC2s on imaging cytometry. (**H**) In vitro–generated and sorted cDC2s were stimulated with iFN- α and medium or OVA in different complexes and cocultured with OVA-specific CD4$^+$ T cells. Four days later, T cell proliferation was read out (left), and IL-2 and iFN-γ production was quantified in the supernatants (right). (**I**) B cells in blood, spleen, or liver at day 7 posttreatment with anti-mouse CD20 antibodies in different formats, expressed as percentage of live CD45$^+$ cells measured by flow cytometry. n.s., not significant. (**J**) Temperature curves of FcεR1γ$^{-/-}$, wild-type, or hFcγR^{ki} mice after intravenous administration of 0.5 mg of human heat-aggregated IVIgs. (**K** and **L**) Ex vivo ADCC by NK cells from hFcγR^{ki} or C57Bl/6N spleens, stimulated with wild-type or afucosylated human IgG1 anti-CD20 antibodies (rituximab or obinutuzumab, respectively) (K) or with multifunctional antibody-based NK cell engagers (l). ADCC was read out as the percentage of maximal ^{51}Cr release from tumor cells. (**M**) hFcγR^{ki} mice intravenously received CD20- expressing B16.F10 melanoma cells and multifunctional nK cell engagers 1 day later. metastasis formation was determined as the proportion of lung affected by metastasis at day 14. (**N**) Levels of monospecific IgG1 (%) with or without abrogated binding to FcRn after concomitant administration with IVIgs in hFcγR/hFcRn^{ki} mice. Each point represents a biological replicate, and histograms were adjusted to their respective modes. confidence intervals represent the standard error of the mean. *P* values were calculated via Mantel-Cox log rank test [(B), left] or one- way ANOVA with Dunnett's [(H), (I), and (M)] or tukey's [(B), right] correction for multiple testing.

We studied NK cell–mediated ADCC to gain insights into the functionality of hFcγRIIIA. In the presence of anti-C D20 antibodies, NK cells purified from hFcγR^{ki} mouse spleens exhibited increased killing efficiency of CD20- expressing melanoma cells, as compared with wild-t ype NK cells (Fig. 6K). ADCC was more potently induced by the afucosylated antibody obinutuzumab than by chimeric antibody rituximab, consistent with afucosylation enhancing hFcγRIII binding. Tumor killing was further improved after stimulation with a multifunctional and Fc optimized NK cell engager, which links both NKp46 and hFcγRIII to an antigen of interest (Fig. 6L) (86, 87). In line with these in vitro observations, we noted decreased lung metastasis formation by CD20-expressing B16.F10 melanoma cells after a single dose of multifunctional NK cell engagers, but not after administration of Fc dead or nonoptimized Fcγ receptor therapeutics (Fig. 6M).

To assess the role of human FcRn in extending the half-l ife of human antibodies, we performed an in vivo pharmacokinetic (PK) study. hFcγR/hFcRn^{ki} mice were administered human IVIgs along with a monospecific human IgG1, either with or without IHH substitutions (I253A/H310A/H435A) that disrupt FcRn binding (Fig. 6N) (88). Demonstrating the functionality of human FcRn, we observed a faster clearance of the IHH-modified antibodies compared with the wild- type antibodies because of decreased FcRn- mediated recycling. Together, these results highlight the utility of hFcγR/hFcRn^{ki} mice in modeling PK.

DISCUSSION

Effector functions of IgG antibodies include cell activation or inhibition via Fcγ receptors and initiation of the complement cascade. Another key function of the Fc tail of IgG is antibody trafficking and recycling via FcRn. For optimizing therapeutic use of antibodies, IgGs are frequently manipulated to engage Fcγ receptors differentially either via selection of a specific IgG antibody subclass and/or Fc engineering (20). Preclinical modeling of therapeutic responses and toxicities of these variant IgGs

Published in : Sci. Immunol (2026), vol. 11, n°115
DOI: 10.1126/sciimmunol.ady7328
Status : Postprint (Author's version)

remains a hurdle, caused by significant disparities between model organisms and humans in Fc receptor genetic and expression profiles. To mitigate these problems in preclinical research, we provide a comprehensive comparison between human, macaque, and mouse Fcγ receptor expression and introduce a humanized mouse model in which humanized Fcγ receptors are expressed under the control of their unique regulatory elements.

Our comprehensive mapping evaluated Fcγ receptor and FcRn expression across cell types, tissues, and species, both at the protein (Fig. 7) and mRNA levels. Among the mentioned discrepancies, the following are noteworthy: (i) Humans and macaques have only one high- affinity activating Fcγ receptor (FcγRI), whereas mice have two receptors that bind to monomeric IgGs (mFcγRI and mFcγRIV) with high affinity; (ii) human and cynomolgus macaque cDCs harbor activating Fcγ receptors, whereas mouse cDCs express inhibitory receptors in steady state; (iii) mouse NK cells express low levels of mFcγRIII, which adds to their decreased ability for ADCC as compared with human NK cells (89); (iv) cFcγRIII is not found on macaque granulocytes (90), in contrast with its expression on human and mouse granulocytes; and (v) human IgGs administered to mice exhibit extended half- lives relative to mouse IgGs because of the higher affinity of mFcRn for human IgG (72), although their half- lives remain shorter than those in humans (91).

A better understanding of how Fc receptor expression is shaped during inflammation is critical for deciphering antibody- driven diseases and optimizing monoclonal antibody therapies. To address this, we systematically analyzed how cytokines modulate Fcγ receptor expression profiles in humans and mice. Although the importance of antibody effector responses in host defense is well established, it was, nevertheless, remarkable that all tested stimuli significantly altered Fcγ receptor transcription in human PBMCs and that numerous mouse cytokines exerted similar effects. This dynamic, cell-t ype–specific regulation points to substantial genomic flexibility, which we explored by (i) querying a prior knowledge model (NicheNet) and (ii) integrating orthogonal evidence from TF prediction using combined single-c ell assay for transposase-accessible chromatin (scATAC)– and scRNA-seq analysis (SCENIC+), supported by ChIP-s eq and perturbation experiments. This approach not only provided some informative insights (e.g., for *FCGR2A*) but also underscored technical challenges arising from copy number variations in the human low-affinity Fcγ receptor locus (5). Because short- read sequencing approaches cannot confidently assign reads from highly homologous genomic regions, standard pipelines exclude many potentially informative signals.

These copy number variations explain the apparent absence of open chromatin at TSSs, such as *FCGR2B* in B cells or *FCGR3A* in NK cells, despite robust expression. These artifacts not only limit accurate inference of TF binding but also complicate our cross- species TF comparison, because multimapping- related filtering does not occur in mice where the duplications are absent. Moreover, SCENIC+ predictions may partly capture lineage-r elated transcriptional programs rather than direct regulation of Fcγ receptors, which likely accounts for some of the divergence with NicheNet predictions. For these reasons, we present the results of each approach in parallel, emphasizing their complementary, exploratory value rather than integrating them into a unified compendium. Ultimately, a definitive reference of transcriptional networks controlling Fcγ receptor expression will require long-ead–based datasets. Until such resources become available, we believe that the combination of evidence from predictions, TF binding data, and perturbation studies can serve as a foundation for future work.

Published in : Sci. Immunol (2026), vol. 11, n°115
DOI: 10.1126/sciimmunol.ady7328
Status : Postprint (Author's version)

An approach to address these interspecies differences and foster the development of therapeutic antibodies is with mice harboring humanized Fcγ receptors. Such mouse lines have been created previously (21–26) and have been crossed to other strains to limit the formation of antidrug antibodies (92, 93) and improve antibody trafficking (27, 93) (summarized in data file S13). In addition to a more human- like expression profile, a benefit of such models is that antibodies do not need to be reformatted into a murine Fc backbone before in vivo evaluation. Our approach builds on previous humanization efforts and addresses several of their limitations, such as random integration of human transgenes and positional effects (21), supernumerary gene copy numbers (30), and limited commercial availability (22, 24). Our extensive characterization of the knockin receptors revealed an expression pattern that was largely in line with that observed in humans (3, 32), and they retained responsiveness to cytokine-induced regulation. However, differences do remain: (i) Classical monocytes from hFcγR^{ki} mice displayed lower amounts of hFcγRI surface staining compared with their human counterparts; (ii) DCs in lymphoid tissues of hFcγRki mice expressed hFcγRIIB, rather than hFcγRIIA in humans; (iii) basophils lacked hFcγRIIA and hFcγRIIB expression, although their expression could be induced in vitro by IL-3 ; (iv) although hFcγRIIIA expression on NK cells was incomplete in hFcγR^{ki} mice, it remained functional and enabled robust ADCC activity compared with that in wild-t ype mouse NK cells; and (v) humanized FcRn in hFcγR/hFcRn^{ki} mice was not expressed by neutrophils (8), likely because of the use of the murine rather than the human promotor.

Fig. 7. Protein expression profiles of Fcγ receptors in humans, macaques, mice, and humanized mice. (**A**) Flow cytometry results of whole blood of healthy human individuals, including cell surface FcRn expression. (**B**) Surface mFcγ receptor and intracellular mFcRn expression in wild- type V57Bl/6J mice, measured by flow cytometry. (**C**) CyTOF data of Fcγ receptors in the whole blood of cynomolgus monkeys (*69*). (**D**) Expression of knockin humanized Fcγ receptors in the hFcγR^{ki} mouse model. The size and color of each data point represent the average of the MFIs across at least three biological replicates, after correction for the negative control and scaling per marker. For cynomolgus monkeys, expression was scaled across the entire dataset because of absence of a negative control.

Published in : Sci. Immunol (2026), vol. 11, n°115
DOI: 10.1126/sciimmunol.ady7328
Status : Postprint (Author's version)

These discrepancies in our knockin mice are in line with those observed in other humanized Fcγ receptor mouse models (21, 22). Beyond their expression, we validated the functionality of humanized Fcγ receptors, showcasing their broad applicability in the development of antibody- based drugs. Hence, we anticipate that our extensive efforts to create, characterize, and validate this mouse should lead to its widespread adoption in preclinical antibody research.

Limitations of the model need to be considered. First, although the hFcγR/hFcRn^{ki} mouse model enables the modeling of native interactions between human antibodies and their receptors, targeted epitopes on proteins of interest might not be shared between mouse and humans, thus requiring further genetic or Fab changes to fully model effector responses. For this purpose, hFcγR^{ki} mice have been crossed to different humanized target epitopes models, such as CTLA-4, VISTA, and CD47. Second, our mouse model is unlikely to mirror the full spectrum of Fcγ receptor–mediated responses seen in humans (6), given that we chose to introduce low- affinity Fcγ receptor alleles. Fcγ receptors exhibit considerable genetic variation driven by evolutionary pressure (15). To circumvent this limitation, additional alleles (FcγRIIA^{H131} and FcγRIIIA^{V158}) are being incorporated into a new generation of humanized models. Further improvements to this model will include the humanization of IgG1 and serum albumin to increase immune tolerance to human IgG1 therapeutics and facilitate the evaluation of drugs that exploit albumin binding to improve half- life. Albumin humanization is warranted to further improve PK-pharmacodynamic studies because mouse serum albumin has a supraphysiologic binding affinity to hFcRn, potentially interfering with FcRn biology (71). Third, differences between IgG- induced complement responses in humans and mice might still affect experimental results (19). Additional differences between human and murine immune functions also remain, and this model does not overcome all translational limitations inherent to preclinical modeling.

As a final caveat, the expression of Fcγ receptors is often used to discriminate myeloid cell types like macrophages and cDCs (59, 94). Our data show that Fc receptors are highly inducible by multiple cytokines, whereas binding- induced internalization greatly reduces surface expression. Fc receptor expression, therefore, is often only useful to delineate cells in steady state. Cross- species differences in receptor expression furthermore preclude the translation of universal gating strategies across species.

In summary, our comprehensive survey of Fcγ receptor dynamics and regulatory elements emphasizes the limitations of wild- type mice and macaques as suitable preclinical models for antibody research. Humanized mouse models, such as the one that we introduce and extensively validate here, can overcome some of the limitations of preclinical research and foster alignment with human physiology and thus rationalize development of therapeutic antibodies.

MATERIALS AND METHODS

Study design

The first aim was to construct an extensive resource of Fcγ receptor expression in humans and in widely used model organisms (mice and cynomolgus macaques). While Fcγ receptor functions depend on protein expression, detection at the cell surface (using flow or mass cytometry) might be

Published in : Sci. Immunol (2026), vol. 11, n°115
DOI: 10.1126/sciimmunol.ady7328
Status : Postprint (Author's version)

confounded by factors such as receptor internalization, low protein abundance, or cytokine or niche-induced modulation of expression. To circumvent this, we generated and mined publicly available omics data across organs, species, and during perturbations and studied various prior knowledge models for cell- cell communication and GRNs involved in Fcγ receptor expression.

To improve the preclinical modeling of therapeutic antibodies and address interspecies differences, the second aim was to generate genetically modified mice expressing all key humanized Fcγ receptors including FcRn instead of their murine counterparts. To characterize these mice, we mapped the expression of knockin receptors using flow cytometry and tested various Fcγ receptor dependent functions (including FcγRI- dependent antigen uptake and presentation, FcγRIIA- dependent mediator release, and FcγRIIIA- dependent cytotoxicity).

Recombinant protein production, fluorescent labeling, and IC formation

Anti- OVA antibodies [Fabs from clones 27_6 and 23_9 (*46*)] were expressed and purified at Evitria SA (Switzerland) with either a wild- type or L234A/L235A/P329G (LALAPG) human IgG1 backbone. Antibodies were expressed in Chinese hamster ovary cells, and the conditioned supernatant was purified in a two-s tep procedure (affinity purification on a MabSelect SuRe protein A resin and size exclusion chromatography on a HiLoad Superdex 200- pg column). Antibodies were buffer exchanged to PBS supplemented with 100 mM l- arginine (pH 6.5 to 6.7) and were filter sterilized. OVA- ICs were generated by incubating two different anti- OVA monoclonal antibodies [clones 27_6 and 23_9 (*46*)] with AF647-labeled OVA in a 1:1 molar ratio for 30 min at room temperature (RT).

The Fab fragment of Synt- 002 (60, 95), used to stain human FcRn, was equally expressed and purified at Evitria SA (Switzerland). Argx 113 was used to stain for murine FcRn, which was expressed and purified at Lonza (Switzerland; batch P63505A).

Proteins were fluorescently labeled as follows. Antibodies in Dulbecco's phosphate- buffered saline (DPBS; Lonza, 17-5 12Q) at 2 mg/ ml were buffer exchanged into 100 mM $NaHCO_3$ (pH 8.3) with Zeba Spin Desalting Columns (Thermo Fisher Scientific, 89893) according to the manufacturer's instructions. AF647 dyes (Invitrogen, A37573) were prepared at a concentration of 20 mg/ml in anhydrous dimethyl sulfoxide (DMSO; Invitrogen, 2025920). To achieve a degree of labeling of two dye molecules per protein molecule, a twofold molar excess of AF647 dye was added to buffer exchanged protein and incubated for 1 hour in the dark at RT. Then, the mixture was centrifuged at 10,000 rpm at 4°C for 15 min. The supernatant was dialyzed against DPBS for 3 days in the dark at 4°C using a dialysis membrane with 6- to 8- kDa molecular weight cutoff (Spectra/Por 1, 3312928). After dialysis, if size exclusion analyses indicated greater than 1% aggregates, then labeled protein was purified using an NGC Quest 10 Chromatography System (Bio- Rad) and a HiLoad 16/600 Superdex 200- pg column (Cytiva). The labeled protein was filtered through 0.22- μm syringe filters (Olympus, 25- 243) and quantified using a NanoDrop One (Thermo Fisher Scientific). OVA (InvivoGen, 9006-5 9- 1) was fluorescently labeled with AF647 Succinimidyl Ester (Thermo Fisher Scientific, A37573) according to the manufacturer's instructions.

Published in : Sci. Immunol (2026), vol. 11, n°115
DOI: 10.1126/sciimmunol.ady7328
Status : Postprint (Author's version)

Human whole- blood processing and staining

Fresh EDTA- treated blood of healthy volunteers was provided by CRI Zwijnaarde (ethical approval Argx-P O-BV- 2022- 1094). Whole blood was incubated with 10 ml of RBC Lysis Buffer (Invitrogen, 00-4333- 57) for each milliliter of blood during 10 min at RT. Cells were washed twice with cold PBS and counting beads (BioLegend, 424902) were added. Surface staining was carried out in consecutive steps at 4°C for 45 min in 150 μl of staining mix, initially for the activating Fcγ receptors in the presence of Monocyte Blocker (BioLegend, 426103) (96) and subsequently for all other antibodies and viability dye (Invitrogen, 65- 0866- 18) using a mix of 50:50 PBS and Brilliant Stain Buffer (BD, 566349). Clone IV.3 was used at a 1:100 dilution for whole- blood staining, a condition under which FcγRIIA- expressing neutrophils act as a binding sink that minimizes potential cross- reactivity with FcγRIIB as reported previously (32). FcRn was then stained at the cell surface in PBS, followed by a fixation step in 2% paraformaldehyde for 20 min at RT. Intracellular FcRn was stained for 45 min after fixation and permeabilization (Invitrogen, 00- 5523- 00). Fluorescence- minus- one (FMO) controls were prepared using pooled samples for Fcγ receptors (FcγRI, FcγRIIA, FcγRIIB, and FcγRIIIA/B) and FcRn.

Platelets were collected from EDTA-treated whole blood. The platelet- rich plasma fraction was isolated after centrifugation at 200g for 10 min at 4°C, pelleted (800g for 10 min at 4°C), stained as described above, and fixated using 2% paraformaldehyde for 20 min.

Mice

C57BL/6J and C57BL/6N mice were purchased from Janvier (France). Ova- specific $CD4^+$ (OTII) (46) (originally from Charles River, France) mice were bred in- house. Mice lacking the Fc receptor gamma chain (Fcεr1$\gamma^{-/-}$; C57BL/6 J-F cer1g^{em1Irc}/Irc; MGI:7612006) were generated by the Transgenic Core Facility of the VIB- UGent Inflammation Research Center (IRC) by electroporating Cas9 ribonucleoprotein complex with guide sequences 5′- AGGGCGGCTGAGGGGATACA- 3′ [guide RNA 1 (gRNA1)] and 5′- GTAAGTCTTTAACGGAGATG- 3′ (gRNA2). This resulted in an allele with a 1560–base pair deletion between gRNA1 and gRNA2 target sites (chr1:171057288 171058847), removing all coding sequences of the Fcer1g gene (ENSMUSG00000058715), except for exon 1 and expected to result in a null allele. All base annotations were according to C57BL/6J genome assembly GRCm39.

Humanization of FcγRI, FcγRIIA, FcγRIIB, FcγRIIIA, and FcγRIIIB (hFcγR^{ki} or genO- hFcγR; genOway catalog fcγr) was achieved by knockin by genOway, France. Targeting vectors were constructed from genomic C57BL/6N mouse strain DNA and human RP11- 241H1 and CH17-4 37O13 BACs. Constructs encoded for humanized FcγRI, FcγRIIA^{R131}, FcγRIIB^{I232}, FcγRIIIA^{F158}, and FcγRIIIB^{NA2}, while the signaling into mouse cells remained functional. These designs disrupted mFcγRI, mFcγRIIB, mFcγRIII, and mFcγRIV and abrogated their expression. Fcγ receptor promoters used human sequences to achieve a human- like expression pattern. Promoter region sizes were selected on the basis of existing models and experimentally validated data on regulatory elements reported in ENCODE database. The linearized targeting vectors were transfected into C57BL/6N ES cells. Embryonic stem cell clones carrying the humanized FcγRI locus (chromosome 3) and humanized low/ intermediate- affinity cluster (chromosome 1) were isolated, amplified, duplicated, and genotyped by both polymerase chain reaction (PCR) and sequencing. Humanized stem cells were microinjected into C57BL/6N blastocysts and gave rise to male chimeras. Breeding with C57BL/6N Cre-deleter mice (CMV- Cre) led to the

Published in : Sci. Immunol (2026), vol. 11, n°115
DOI: 10.1126/sciimmunol.ady7328
Status : Postprint (Author's version)

excision of the selection cassettes, thus producing the heterozygous FcγRI or FcγRIIA/IIB/IIIA/IIIB humanized mouse lines. These heterozygous animals were validated by both PCR and sequencing. The two lines were then interbred to produce the homozygous hFcγR^{ki} animals reported here.

The hFcγR/FcRn^{ki} or genO- hFcγR/hFcRn line (genOway catalog geno- hfcγr- hfcrn) was generated by interbreeding of the humanized Fcγ receptor mouse line with the humanized FcRn mouse line, described previously (71). Briefly, the humanized FcRn mouse line expresses human FcRn instead of mouse FcRn. Expression of humanized FcRn is driven by the mouse endogenous promoter. Breeding of the two lines generated homozygous humanized mice of which the genotype was validated by both PCR and sequencing.

Unless explicitly mentioned otherwise, all experiments were performed with a mixture of male and female mice. Similar findings were obtained for both sexes, except the drop in body temperature in anaphylaxis, with females being more susceptible as previously shown (97). All animals were maintained at specific pathogen–free conditions in individually ventilated cages with 12- hour day/night cycles. Food and water were provided ad libitum for the duration of the experiments. All in vivo experimental procedures were conducted according to the institutional guidelines and approved by the animal welfare committees of the VIB Center for Inflammation Research (2022- 025 2024- 65), Innate Pharma (APAFIS, 19272), or Washington University in St. Louis (23- 0198).

Mouse sample processing and staining for flow cytometry

Peripheral blood was collected via heart puncture in EDTA- coated tubes. For peritoneal lavage, 6 ml of PBS/EDTA (2 mM) was injected in the flank of the peritoneum and aspirated after gentle shaking. Mesenteric lymph nodes, lung, spleen, and tibia were all collected in cold RPMI (Gibco, 11875093). All samples were kept on ice until processing. EDTA- treated whole blood was washed once, followed by two rounds of red blood cell lysis (Gibco, A1049201) at RT during 1.5 min. Spleen, lung, and mesenteric lymph nodes were cut with scissors into small pieces and digested at 37°C for 30 min in RPMI containing Liberase (20 μg/ml; Roche, 05401127001) and deoxyribonuclease I (DNAse I; 10 U/ml; Roche, 04536282001). Digested samples were passed through a nylon mesh with 70- μm pores (Corning, 431751). BM cells were flushed from tibia with cold RPMI medium and passed over a 70- μm cell strainer. Red blood cells were removed from the BM, spleen, and lung samples using ACK Lysis Buffer (Gibco, A1049201) for 2 min at 4°C. For the analysis of platelets, whole blood was collected via tail bleeding in EDTA- coated tubes, which were kept at RT throughout processing and staining.

Red blood cells were similarly removed in two steps.

Liver cells were isolated by liver perfusion and digestion as described previously (*98*). After retrograde cannulation, livers were perfused for 1 to 2 min with an EGTA-containing solution, followed by a 6 min (6 ml/min) perfusion with collagenase A (0.2 mg/ml; Roche, 11088793001). Livers were then removed, minced, and incubated for 20 min with collagenase A (0.4 mg/ml) and DNase I (10 U/ ml) at 37°C. All subsequent processing was performed on ice. Samples were filtered over a 100- μm mesh filter, and red blood cells were lysed. After another filtration step over a 40- μm mesh filter, samples were centrifuged twice at 50*g* for 1 min to remove hepatocytes (pellet). Cells remaining in the supernatant

Published in : Sci. Immunol (2026), vol. 11, n°115
DOI: 10.1126/sciimmunol.ady7328
Status : Postprint (Author's version)

(including leukocytes and LSECs) were then centrifuged for 5 min at 400g before proceeding to antibody staining for flow cytometry.

Single- cell suspensions were first stained for 45 min with mouse or humanized Fcγ receptors, viability dye (Invitrogen, 65-0 866- 18 or 65- 0865- 14), and biotinylated antibodies. All remaining antibodies for surface staining were next added for 30 min and fixed for 20 min using 2% paraformaldehyde. Where applicable, FcRn was stained intracellularly after fixation and permeabilization (Invitrogen, 00-5 523- 00). Unstained controls for Fcγ receptors or FcRn were created from pooled samples. Fc block [gift from L. Boon (JJP Biologics), clone 2.4G2] was added both intra- and extracellularly to all unstained control samples and to samples stained for FcRn.

With the exception of the platelet staining (37°C), all stainings were carried out at 4°C. Unstained controls were included for all surface Fcγ receptors together, and FcRn intracellularly. All antibodies are listed in data file S14.

Cytokine administration to hFcγR/hFcRn^{ki} mice

We administered 5 μg of cytokines of IFN- α2, IFN- γ, GM- CSF, IL- 4, and IL- 10 (Thermo Fisher Scientific, 14- 8312- 80, 315- 05, 315- 03, 214- 14, and 210-1 0, respectively) dissolved in 100 μl of sterile PBS via the tail vein. After 16 hours, mice were euthanized, and a single- cell suspensions were prepared through enzymatic digestion. Surface staining was performed for hFcγRI, hFcγRIIA, hFcγRIIB/C, and hFcγRIIIA/B. hFcRn was stained intracellularly after fixation and permeabilization.

Flow and mass cytometry data acquisition and analysis

All conventional flow cytometry samples were measured on a BD FACSympony A5, A3, or LSRFortessa 5 laser. Single-s tained beads (Invitrogen, 01- 2222- 42) were prepared to adjust the sensitivity of the photomultiplier tubes and construct a compensation matrix. Spectral flow cytometry samples were measured on an ID7000 (Sony) with each photomultiplier tubes' voltage at maximal saturation. Autofluorescence extraction and spectral unmixing were carried out in the ID7000 Spectral Cell Analyzer (Sony). CyTOF on whole blood of cynomolgus monkey (*M. fascicularis*) (*69*) was accessed from http://flowrepository.org/id/FR- FCM- ZZSR.

Downstream cytometry analysis, including compensation (for conventional flow cytometry only), manual gating, and dimensional reduction, was performed using FlowJo v10.9.0 (BD). Visualization through t- distributed stochastic neighbor embedding was executed using the default parameters, incorporating all channels displaying a bimodal distribution after manual axis transformation in FlowJo. Manual gating strategies are provided across the supplementary figures and in data file S5.

Heatmaps were generated in R v4.3.2 and using the packages dplyr v1.1.4, ggplot2 v3.4.4, FlowSOM v2.10.0, flowCore v2.14.0, and ComplexHeatmap v2.20.0. For steady-state protein expression, the fluorescent channels of interest, manually gated cell types, tissues, individual samples, and workspaces were first identified per analysis. Median fluorescence intensities (MFIs) and cell counts were then extracted across all populations of interest and adjusted for the unstained control through subtraction (any negative values were replaced by zero). The fluorescent intensities were normalized for each marker across each dataset, after which the average expression for each population within each tissue

Published in : Sci. Immunol (2026), vol. 11, n°115
DOI: 10.1126/sciimmunol.ady7328
Status : Postprint (Author's version)

was determined. Due to absence of unstained samples in the macaque dataset, scaling for Fcγ receptor intensities was performed across all markers of interest in the entire dataset. Results were then plotted using the funkyheatmap v0.5.0 package (99).

For the cytokine-induced humanized Fcγ receptor expression analysis, the compensated MFI values were extracted from FlowJo for each population per biological replicate. Data were further processed in R. To ensure that no negative MFI values were present, the lowest below zero (if any) were added per marker. Mann-Whitney U tests and mean $\log_2$ fold changes were computed for each Fcγ receptor and cell type, comparing cytokine-t reated samples to PBS group ($n = 5$ per group). P values were adjusted for multiple comparisons using the Benjamini-Hochberg correction for each cell population per genotype, marker, and stimulus.

High- throughput protein analysis of BM samples

Human and murine BM samples were obtained from a BM aspirate acquired during total hip arthroplasties (University of Liège ethical committee 2022/78) and from C57BL/6J mice, respectively. Single- cell suspensions were stained, processed, and analyzed using an extensive PE- conjugated antibody panel on top of a 12- or 13-color backbone panel, as described previously (35). Single viable $CD45^+$ $dump^{lo/int}$ cells were analyzed with the Infinity Flow pipeline (36), and its output files were further analyzed in FlowJo.

Human gating on human BM was carried out as follows. Basophils and mast cells were identified using manual gating on $CD200R^+$ $CD203c^+$ cells, with mast cells being $cKit^+$ and $CD123^{lo/int}$, and basophils expressing high CD123. Basophils were $CCR3^+$, whereas their progenitors were $CCR3^-$. Eosinophils were selected as $CD84^+$ $CD38^-$ Siglec- 8^+ SSC- A^+ cells. Eo I to Eo IV subsets were identified manually as described (35). Hematopoietic and multipotent progenitors were gated as $CD34^+$ $CD38^-$ cells. Additional $CD38^+$ $CD34^+$ progenitors were further divided into $Fcer1a^+$ basophil and mast cell progenitors and $CD125^+$ eosinophil progenitors. Neutrophils and monocytes were identified as Siglec- 8^- $CD125^-$ $CD15^+$ SSC- A^+ cells, with monocytes expressing CD192 and CD11c.

Murine BM populations were identified as follows. $Lin^-Sca1^+Kit^+$ cells were gated according to their nomenclature with an additional forward and side scatter gate. Basophil and mast cell lineages were gated as $CD55^+CD115^-CCR3^-CD200R3^+$. Within this population, progenitors were defined as c-K it^+Fcer1^-, basophil precursors as c-K it^-Fcer1^-, basophils as c-K it^-Fcer1^+, and mast cells as c- Kit^+Fcer1^+. Eosinophil subsets I to IV were gated manually as described before (35). Neutrophils precursors were identified as $CD55^-$ $CD135^-CD115^-CD93^{lo}$; developing neutrophils further divided using CD11b and DcTRAILR1.

Imaging cytometry

For ImageStream flow cytometry, surface markers (XCR1, CD11c, and CD11b) and Fixable Viability Dye eFluor 780 (Invitrogen, 65- 0865- 14) were stained on BM-derived DCs after which the cells were washed, fixed, and permeabilized (BD, 554714), allowing for intracellular staining with antihuman CD32a, CD64, CD32b, and CD16. After washing, the cells were analyzed on a ImageStreamX MkII

Published in : Sci. Immunol (2026), vol. 11, n°115
DOI: 10.1126/sciimmunol.ady7328
Status : Postprint (Author's version)

(Cytek) equipped with INSPIRE software. Compensation was carried out using beads (Invitrogen, 01-2222- 42). The data were analyzed using IDEAS software (Millipore).

Immunoglobulin and cytokine detection

Serum immunoglobulins were measured by enzyme- linked immunosorbent assay (ELISA) in serum in half area plates (Greiner, 675061). In brief, wells were incubated with 50 μl of coating antibodies overnight at 4°C and blocked with 150 μl of 1% casein (Merck, C7078) in PBS for 2 hours. Samples were diluted in 0.1% casein buffer (IgA, 1/200; IgM, 1/3200; IgE, 1/5; and IgG, 1/30,000). Samples (50 μl) or standards were incubated for 2 hours at RT on an orbital shaker. Afterward, detection antibodies were added for 1 hour. After thorough washing, 50 μl of development substrate (Invitrogen, 00- 4201- 56) was added, and the reaction was stopped using 25 μl of 1.25 M sulfuric acid (VWR, 20700.298). IL-2 and IFN-γ in the supernatant of the OTII- cDC2 cocultures were quantified by ELISA (dilution IL-2 , 1/5; and IFN- γ, undiluted) according to the manufacturer's instructions (Invitrogen, 39- 50400- 65 and 88-7 024- 88). Absorbances at 450 and 650 nm were measured using a Tecan Infinite M Plex reader.

Histology

The postcaval lung lobe, left kidney, and right lateral liver lobe were placed overnight in 4% paraformaldehyde and embedded in paraffin. Five-micrometer- thick sections of lung and liver and 3-μm- thick kidney sections were stained with hematoxylin and eosin (Leica Autostainer ST5010).

BM- derived cell cultures and DC–T cell cocultures

BM was isolated from both femurs and tibias. After incubation with 70% ethanol, bones were smashed in a mortar and filtered through a nylon 100- μm strainer at 4°C. Cells were resuspended in 10% DMSO, 45% fetal bovine serum, and 45% tissue culture medium [consisting of RPMI 1640, 10% fetal bovine serum (Tico, FBSEUXXX, batch 90439), 0.1% 2-mercaptoethanol (Sigma- Aldrich, M3148), 1% l- alanyl- l- glutamine dipeptide (Gibco, 35050038), and 0.5% gentamicin (Gibco, 15710049)]. BM cells were slowly cooled to −80°C (Thermo Fisher Scientific, 5100- 0001) and then stored at −150°C.

Basophils and mast cells were cultured from frozen BM. BM cells (4×10^6) were seeded in 2 ml of tissue culture medium with recombinant IL- 3 at 5 ng/ml (PeproTech, 213-1 3) in 24-well plates. Cells were maintained at 37°C in a humidified atmosphere at 5% CO_2. Medium was changed every 3 days, and cells were split at day 7. Flow cytometry was carried out on day 9, and populations were identified as previously shown (100).

DCs were cultured out as described previously (46). In brief, frozen BM was thawed, seeded at 2×10^6 cells per 2 ml in 24- well pates, and cultured in tissue culture medium (see above) with human FLT3L (250 ng/ml; recombinant, VIB Protein Core). Enhanced green fluorescent protein–OP9 feeder cells (*101*) (CVCL_B218; gift from T. Taghon) were grown in minimum essential medium (Gibco, 22571- 020) supplemented with 20% fetal bovine serum, 0.6% gentamicin, and 1.2% l- alanyl- l- glutamine dipeptide. On day 3 of the DC culture, DCs were transferred to wells containing a monolayer of OP9 cells. On day 8, the 50:50 DC:OP9 medium was refreshed, and 100 ng of IFN- α (gift by R.

Published in : Sci. Immunol (2026), vol. 11, n°115
DOI: 10.1126/sciimmunol.ady7328
Status : Postprint (Author's version)

Vandenbroucke), ICs (with OVA at 3 or 10 μg/ml, and antibodies in a 1:1 molar ratio), and FLT3L (250 ng/ ml) were added. Twenty hours later, DCs were harvested for flow cytometry or cell sorting.

Naive OVA- specific T cell receptor–transgenic $CD4^+$ T cells were isolated from mechanically disrupted, filtered, and red blood cell– depleted spleen and lymph nodes. The presence of Vα2 and Vβ5 T cell receptors on $CD4^+$ T cells was confirmed before cell sorting. T cells were labeled with CellTrace Violet (Invitrogen, 65- 0842- 90) and before cell sorting. OTII cells (100,000) were incubated with 10,000 sorted cDC2s in 200 μl of tissue culture medium, in a 96- well plate. All samples were kept at 37°C with 5% CO_2. After 4 days, samples were spun down, and 170 μl of supernatants was collected for ELISAs. Cells were stained in 50 μl at 4°C, washed, and evaluated using flow cytometry.

Fluorescence- activated cell sorting

For scRNA-seq, six spleens of female C57BL/6J mice (Janvier, France) were processed as described above. Single- cell suspensions were sorted on a BD FACSymphony S6. To isolate different immune cells spiked in equal numbers, the single- cell suspension was enriched by depleting $CD3e^+$ and $CD19^+$ cells using biotin-labeled monoclonal antibodies and MagniSort Streptavidin Negative Selection Beads (Thermo Fisher Scientific, MSNB-6 002- 74). $CD3e^+$ and $CD19^+$ cells were sorted from a not enriched fraction of the sample. T cells ($CD3e^+$), B cells ($CD19^+$), basophils ($CD200R3^+$ $Fcer1^+$ $CD45^{dim}$), innate lymphoid cells (ILCs) ($CD3e^-$ $CD127^+$ $CD90.2^+$), macrophages ($F4/80^+$ $CD64^+$), NK T cells ($CD3e^+$ $CD161^+$), NK cells ($CD3e^-$ $CD161^+$), cDC1s ($CD11c^+$ $MHCII^+$ $XCR1^+$), cDC2s ($CD11c^+$ $MHCII^+$ $CD172a^+$), neutrophils ($CD11b^+$ $Ly6G^+$), monocytes ($CD11b^+$ $Ly6G^-$ $Ly6C^+$), eosinophils ($CD11b^+$ $SiglecF^+$), pDCs ($CD11b^-$ $Bst2^+$ $Ly6C^+$), and mast cells ($Fcer1^+$ $CD117^+$ $CD11c^-$) were sorted, centrifuged, and resuspended in Rhapsody buffer (BD, 650000062).

For cDC2 and OTII cocultures, FLT3L- stimulated BM cultures were filtered, washed, and stained for 30 min at 4°C. Single, viable, $CD11c^+$ $MHCII^+$ $XCR1^-$ $CD172a^+$ cDC2s were sorted on BD FACSAria II or III. OTIIs were identified as single, viable, Lin^- (CD19, CD11c, and MHCII) $CD4^+$ $CD8^-$ $CD62L^+$ cells on a FACSAria II or III.

Influenza infection model

The A/Puerto Rico/8/34 (PR8) H1N1 viruses were obtained from the International Reagent Resource (US Centers for Disease Control and Prevention) and the National Institute for Biological Standards and Control. Propagation of viral stocks was performed as previously described (102).

Prophylactic activities of FY1 Fc variants against A/Puerto Rico/8/34 (PR8) virus infection were performed in 7- to 9-week- old female $hFc\gamma R^{ki}$ mice that were randomized on the basis of age and weight before antibody treatment and virus infection. FY1 Fc variants (2 mg/kg) (82) were administered intravenously 2 days before virus infection. On the day of infection, mice were anaesthetized with 2% isoflurane and intranasally infected with five times the lethal dose 50 (5× LD_{50}) of viruses diluted in 50 μl of PBS. After infection, mice were monitored daily, and their weights were recorded. Mice were euthanized when 30% weight loss occurred per the IACUC regulations. Weight curves were assessed by comparing the area under the curve of the weight loss over time using a one-w ay analysis of variance (ANOVA).

Published in : Sci. Immunol (2026), vol. 11, n°115
DOI: 10.1126/sciimmunol.ady7328
Status : Postprint (Author's version)

Twenty- four hours after dosing, serum was collected from each mouse for quantification of human FY1 IgG Fc variants using the Meso Scale Discovery (MSD) platform. MSD plates were coated overnight with mouse antihuman CH2 capture monoclonal antibody, washed three times, and blocked using 5% bovine serum albumin. Serum samples, standards, and quality control samples (prepared in pooled mouse serum) were added to the plate using a minimal required dilution of 50 and incubation for 60 min while shaking. After further washes, ruthenium-labeled goat antihuman IgG polyclonal antibody was added for detection. After adding MSD GOLD Read Buffer A, electrochemiluminescence signals were acquired using the Meso QuickPlex SQ 120 plate reader (MSD). Human IgG in samples was quantified against FY1 standards using four- parameter logistic curve fitting.

B cell depletion model

hFcγR^{ki} male mice were injected with a single retro-o rbital intravenous dose (250 μg per mouse) of anti-m ouse CD20 monoclonal antibody [18B12 (83), mouse IgG2a], human IgG1 isotype control (MSL109), or anti- mouse CD20 on a human IgG1 backbone with or without additional Fc engineering. For the quantification of B cell numbers, blood was collected in EDTA-coated tubes by heart puncture on day 7 after anti- CD20 treatment. Spleens and livers were also harvested on day 7 posttreatment and enzymatically dissociated before being stained. B cell depletion was evaluated using flow cytometry, and the number of CD45$^+$CD19$^+$CD3$^-$ cells was plotted as a percentage of total CD45$^+$ cells.

Heat-aggregated human immunoglobulins (passive systemic anaphylaxis)

Aggregated human IVIgs were generated as previously described (22). Immunoglobulins (25 mg/ml; Privigen) were dissolved in borate- buffered saline [0.17 M H_3BO_3 (Merck, 1007650050) and 0.12 M NaCl (Merck, 1064060250) at pH 8] and incubated at 63°C for 1 hour. Next, ICs were further diluted to 0.5 mg/100 μl in 0.9% NaCl and injected intravenously via the tail vein. Rectal temperatures were followed for 90 min after injection.

B16.F10 melanoma cell transfection

B16.F10 cells (ATCC; CRL- 6475) were transfected to express human CD20 (NP_068769.2), which was inserted into a SLX expression vector between the Hind III and Xba I restriction sites. After sequencing, the vector was used to transfect the B16- F10 cell line with AMAXA Nucleofector 4D technology. The cells were cultured under selection with hygromycin (50 mg/ml). Positive cells, stained with an anti-CD20 fluorescein isothiocyanate antibody, were sorted. The cell line was cultured in RPMI 1640 medium supplemented with 10% heat- inactivated fetal bovine serum, 2 mM l- glutamine, 1% nonessential amino acids, and 1 mM sodium pyruvate (all from Gibco) and maintained at 37°C under an atmosphere containing 5% CO_2.

Ex vivo NK cell assays

Mouse NK cells were purified from spleen of C57BL/6N (Charles River, France) or hFcγR^{ki} female mice, using Mouse NK Cell Isolation Kit (Miltenyi, 130- 115- 818). Several therapeutics were tested: obinutuzumab (Roche), rituximab (Roche), and different anti-C D20 antibody- based NK cell engager

Published in : Sci. Immunol (2026), vol. 11, n°115
DOI: 10.1126/sciimmunol.ady7328
Status : Postprint (Author's version)

therapeutics (Innate Pharma). These NK cell engagers contain various building blocks: a Fab fragment recognizing human CD20, a human IgG1 Fc, and a Fab fragment anti- mouse NKp46 or an irrelevant Fab. The IgG1 Fc fragment was either wild type, mutated to abolish binding to Fcγ receptors (Fc dead, N297S), or mutated to enhance binding to Fc receptor (Fc opt, S239D and I332E).

NK cells were plated with human $CD20^+$ B16.F10 tumor cells loaded with 50 μCi/10^6 cells of chromium-51 (^{51}Cr; PerkinElmer) at an effector:target cell ratio of 10:1 in U-bottom 96-well plates (BD Falcon). Dose ranges of test molecules were added (in duplicate), and plates were incubated for 4 hours at 37°C in RPMI 1640 medium supplemented with 10% heat- inactivated FBS, 2 mM l- glutamine, 1% nonessential amino acids, and 1 mM sodium pyruvate (all from Gibco). After incubation, 50 μl of the culture supernatant was transferred to a LumaPlate (Perkin Elmer) coated with solid scintillator and read with a microplate scintillation counter (TopCount NXT, Perkin Elmer) to measure ^{51}Cr release into the supernatant. The specific lysis was calculated as follows

$$\text{Specific lysis (\%)} = \frac{\text{experimental release} - \text{spontaneous release}}{\text{maximal release} - \text{spontaneous release}} \times 100$$

Maximal ^{51}Cr release was determined by adding 2% Tergitol (Sigma-A ldrich, 15S9) to the target cells, and spontaneous release was measured in medium alone, without effector cells.

In vivo disseminated mouse tumor model

$hCD20^+$ B16.F10 cells (10^6) were injected intravenously into the tail vein of $hFc\gamma R^{ki}$ male and female mice. The indicated treatments (100 μg) were injected intravenously on the following day (8 mice per treatment group). Mice were observed daily to monitor clinical signs and euthanized 13 days after tumor cell inoculation, and the lungs were analyzed for the presence of metastases. A random forest model was built (Trainable Weka Segmentation plugin in Fiji) to distinguish between metastatic and healthy areas. For each sample, the proportion of metastatic area was quantified.

In vivo pharmacokinetic study

Five mixed gender $hFc\gamma R/hFcRn^{ki}$ mice per group received a mix of IVIg (40 mg/kg) and test item (Mota-hIgG1- WT or Mota- hIgG1- IHH, at 40 mg/kg) intraperitoneally. All animals were preweighted before dosing and dosed according to their body weights. Blood of mice was sampled via the tail vein considering the maximum allowed blood volume for multiple collections within 14 days on the following time points: day 0 (1 and 6 hours after test item injection), day 1, day 2, day 4, day 7, day 10, day 14, day 21, and day 28 (terminal) after test item injection. After blood collection, sera were prepared and frozen until further analysis. Test item serum levels (pharmacokinetics) were evaluated on every bleeding time point using an in-house developed ELISA assay.

Size exclusion–high- performance liquid chromatography Analytical SEC-H PLC on OVA-ICs was performed using a LC 1260 System enhanced (Agilent) equipped with Quaternary pump, thermostated column compartment, standard autosampler, and multiple wavelength detector. Samples were

Published in : Sci. Immunol (2026), vol. 11, n°115
DOI: 10.1126/sciimmunol.ady7328
Status : Postprint (Author's version)

analyzed using a XBridge BEH 450 Å–SEC 3.5 μm, 7.8 mm–by–300 mm column (Waters, 176003596) with preguard XBridge BEH 450 Å–SEC 3.5 μm, 7.8 mm–by–300 mm column (Water, 186007641) in DPBS (pH 7 to 7.4; Sigma- Aldrich, D8537) at a flow rate of 0.30 ml/min using 214- and 280- nm wavelength.

In- house–generated scRNA- seq data

The sorted immune cells were resuspended at an estimated concentration of 2000 cells/μl and loaded on a BD Rhapsody cartridge with a targeted capture of 15,000 cells. Reverse transcription, cDNA amplification, and library construction were performed following the manufacturer's instructions [23-24117(02)]. Libraries were sequenced on a NovaSeq6000 flow cell (Illumina).

The BD Rhapsody Sequence Analysis Pipeline (BD, v1.9.1) was used to map the FASTQ files to the mouse reference genome (mm10- 2020- A). Single- cell analysis was performed using RStudio (R version 4.0.5) starting from RSEC_MolsPerCell.csv [data table containing molecules per gene per cell based on RSEC (recursive substitution error correction)].

Preprocessing of the RNA unique molecular identifier matrix was done according to the workflow as previously described (*46*). Outliers were identified based on three metrics: number of expressed genes, library size, and mitochondrial proportion. Cells of 5 median absolute deviations (MADs) away from the median value were filtered out for the number of expressed genes, and library size of 5 MADs was used as an upper limit for the mitochondrial proportion.

The subsequent count matrix was used to create a Seurat Object with the Seurat R package v4.0.5. Count normalization, detecting highly variable genes, and scaling were performed with the SCTransform function with default parameters. Finding clusters and creating Uniform Manifold Approximation and Projection (UMAP) plots was done using the Seurat pipeline. Clustering was performed using the first 35 principal components and a resolution of 1. The final Seurat object contains 7939 cells and 18 annotated clusters. Marker analysis of the different cell clusters was performed using the Wilcoxon rank- sum test with the FindAllMarkers function.

Public single- cell RNA-s eq and bulk RNA-seq data

Tabula Sapiens (39) single- cell datasets (endothelial, stromal, epithelial, and immune) were downloaded from https://figshare.com/projects/ Tabula_Sapiens/100973. Human DC datasets (*42*) were loaded from https://singlecell.broadinstitute.org/single_cell/study/SCP43/ atlas- of- human-blood- dendritic- cells- and-monocytes. Single- cell sequencing results from cultured PBMCs exposed to several stimuli (48) were retrieved via https://zenodo.org/records/15744698. Full-l ength Smartseq2 single- cell data from the Tabula Muris (62) was assessed in R via ExperimentHub v2.4.0. The full nonhuman primate cell atlas (70) was downloaded from https://db.cngb.org/nhpca/download. Conversion of h5ad files to Seurat objects was carried out using the anndata v0.7.5.6 and SeuratDisk v0.0.0 packages in R v4.2.1. Where required, datasets were merged and preprocessed in Seurat v4.4.0, and provided or published annotations were simplified. For the Tabula Muris, organs without immune cells were omitted from downstream analysis. Bulk RNA-

Published in : Sci. Immunol (2026), vol. 11, n°115
DOI: 10.1126/sciimmunol.ady7328
Status : Postprint (Author's version)

s eq data from common γ chain cytokines (65) were downloaded from https://doi.org/10.1084/jem.20222052 (table S3).

Cytokines and prior knowledge networks

Cytokine effects on Fcγ receptor expression were assessed by scRNA- seq on in vitro–cultured PBMCs (https://zenodo.org/records/ 15744698). Mean expression values were calculated for each Fcγ receptor across cell types, stimuli, and biological replicates and compared to baseline using the Wilcoxon test. Conditions with fewer than three cells or an mean expression of <0.1 were excluded as not representative or biologically relevant. P values were adjusted for multiple testing per Fcγ receptor using the Benjamini- Hochberg method. We also queried CytoSig database (49) (https://cytosig.ccr.cancer.gov/), which compiled human cytokine–induced transcriptional changes. Both ligands and GRNs involved in Fcγ receptor expression were equally extracted from NicheNet 2.0 (50, 51) (https://doi.org/10.5281/ zenodo.5884439), which models cell-c ell communication based on large- scale integrated ligand- to- target data. We plotted the 25 ligands with the highest regulatory potential (which quantifies the ability to modulate the expression of a given target) across all Fcγ receptors and the top 10 TFs per individual Fcγ receptor with the highest regulatory potential. Kinases involved in IgG:Fcγ signaling were studied using the model provided in decoupleR (43). Cytokines that alter the transcription of mouse Fcγ receptors were investigated from the Immune Dictionary (63) [for absolute changes, www.immune-dictionary.org/app/ home: log fold changes, table S3 (63)].

TF regulatory potential scoring

For the calculation of the regulatory potential of a TF for a gene, we adapted the regulatory potential model as described by Chen *et al.* (67). Briefly, for a given gene, the regulatory potential of a TF was calculated as the sum of the nearby binding sites weighted by the distance from each site to the annotated TSS of the gene. This model relies on two assumptions supported by experimental observations: First, the regulatory effect of a binding site typically diminishes monotonically with increasing distance of the binding site to the TSS, and, second, the contribution of each binding site is independent of the others so that the influence on a gene is represented by the sum of their individual contributions. A Python script, implementing Chen's model specifications (67), was developed that calculates the regulatory potential score of a TF for a given gene in either the human (hg38) or mouse (mm10) genome. The script takes as input the gene of interest, the species (hg38 or mm10), and the decay distance (1, 10, or 100 kb). Source code is available at https://github. com/pieterdb60/regpot-single- gene. As source of ChIP-Seq TF binding data, the ReMap 2022 database (66) was used.

GRN analysis and its validation on perturbation and ChIP- seq experiments from Encode

Human simultaneous scATAC and scRNA-s eq (Multiome) PBMC data were retrieved and analyzed as previously described (53). In brief, data were retrieved from https://cf.10xgenomics.com/ samples/cell-arc/1.0.0/pbmc_granulocyte_sorted_10k/pbmc_ granulocyte_sorted_10k_filtered_feature_bc_matrix.h5 and https://

Published in : Sci. Immunol (2026), vol. 11, n°115
DOI: 10.1126/sciimmunol.ady7328
Status : Postprint (Author's version)

cf.10xgenomics.com/samples/cell- arc/1.0.0/pbmc_granulocyte_ sorted_10k/pbmc_granulocyte_sorted_10k_atac_fragments.tsv.gz. After quality control, doublet removal, and annotation of scRNA- and scATAC-s eq data, we carried out motif enrichment using pycisTarget and the default SCENIC+ workflow (see https://scope. aertslab.org/#/scenic-v2). From the SCENIC+ output, we then selected Fc receptors and TFs and visualized predicted region- to- gene links.

Next, to evaluate whether TFs predicted by SCENIC+ affected gene expression of Fcγ receptors, we analyzed perturbation experiments from ENCODE deeply profiled cell lines (54). As described previously (53), we calculated $\log_2$ fold change between control and intervention samples using DESeq2 (103) and filtered experiments where Fc receptor expression changed significantly ($P_{\text{adj}} < 0.05$) (see data file S4).

To differentiate between direct and indirect TF activity on Fc receptor expression, we evaluated the presence of binding sites of implicated TFs in the respective cell lines. For this purpose, we downloaded the default bed narrowPeak files from the ENCODE portal (54, 104, 105) with the following identifiers: ENCSR000EGR, ENCS-

R000BKT, ENCSR000EWM, ENCSR000EWG, ENCSR000E HJ, ENCSR000FBC, ENCSR000BRR, ENCSR338UQU, ENCSR031URL, ENCSR258SXK, ENCSR922MQU, and ENCSR734CRN. We overlaid ChIP-seq peaks with the pseudobulk ATAC-s eq data of human PBMCs and region- to- gene expression correlation results from SCENIC+, using Signac v1.13.0, EnsDb.Hsapiens.v86 v2.99.0, GenomicRanges v1.56.0, and rtracklayer v1.64.0 in R.

Data analysis and visualization

All data wrangling was carried out in R using the tidyverse v2.0.0 packages. Visualizations were enabled by the tidyverse, Seurat, Signac, ComplexHeatmap v2.12.1, ggridges v0.5.4, ggpubr v0.6.0, and ggVennDiagram v1.5.2 tools (106).

Hierarchical *k*- mer–based tree

Fcγ receptor sequences were downloaded from the Ensembl Release 110. The construction of a distance-b ased phylogenetic tree was carried out in CLC Main Workbench 20.0.4 (QIAGEN), using the k- mer–based Tree Construction tool with the neighbor joining algorithm, where $k = 15$, and distance measure according to Mahalanobis.

Statistical analysis

Assessing the data distribution was carried out using the Shapiro- Wilk test in GraphPad Prism 10.1.2. For Gaussian distributions, one- way ANOVA testing was performed, with correction for multiple testing using Tukey's test. Nonnormal distributed data were compared using Kruskal- Wallis test with Dunn's multiple comparisons test. All statistical tests were two- sided with an alpha level of 0.05. Where applicable, correction for multiple comparisons was carried out with the Benjamini- Hochberg method.

Published in : Sci. Immunol (2026), vol. 11, n°115
DOI: 10.1126/sciimmunol.ady7328
Status : Postprint (Author's version)

Supplementary Materials

The PDF file includes: Figs. S1 to S7

Other Supplementary Material for this manuscript includes the following:

Data files S1 to S15 mDaR Reproducibility checklist

REFERENCES AND NOTES

1. L. L. Lu, T. J. Suscovich, S. M. Fortune, G. Alter, Beyond binding: antibody effector functions in infectious diseases. Nat. Rev. Immunol. 18, 46–61 (2018).
2. F. Nimmerjahn, J. V. Ravetch, Fcγ receptors as regulators of immune responses. Nat. Rev. Immunol. 8, 34–47 (2008).
3. P. Bruhns, F. Jönsson, Mouse and human FcR effector functions. Immunol. Rev. 268, 25–51 (2015).
4. G. Vidarsson, G. Dekkers, T. Rispens, IgG subclasses and allotypes: From structure to effector functions. Front. Immunol. 5, 520 (2014).
5. S. Frampton, R. Smith, L. Ferson, J. Gibson, E. J. Hollox, M. S. Cragg, J. C. Strefford, Fc gamma receptors: their evolution, genomic architecture, genetic variation, and impact on human disease. Immunol. Rev. 328, 65–97 (2024).
6. S. Q. Nagelkerke, D. E. Schmidt, M. De Haas, T. W. Kuijpers, Genetic variation in low- to- medium- affinity Fcγ receptors: Functional consequences, disease associations, and opportunities for personalized medicine. Front. Immunol. 10, 2237 (2019).
7. P. Bruhns, Properties of mouse and human IgG receptors and their contribution to disease models. Blood 119, 5640–5649 (2012).
8. M. Pyzik, L. K. Kozicky, A. K. Gandhi, R. S. Blumberg, The therapeutic age of the neonatal Fc receptor. Nat. Rev. Immunol. 23, 415–432 (2023).
9. F. Nimmerjahn, J. V. Ravetch, Divergent immunoglobulin G subclass activity through selective Fc receptor binding. Science 310, 1510–1512 (2005).
10. S. B. Mkaddem, M. Benhamou, R. C. Monteiro, Understanding Fc receptor involvement in inflammatory diseases: From mechanisms to new therapeutic tools. Front. Immunol. 10, 811 (2019).
11. A. Pincetic, S. Bournazos, D. J. Dilillo, J. Maamary, T. T. Wang, R. Dahan, B.- M. Fiebiger, J. V. Ravetch, Type I and type II Fc receptors regulate innate and adaptive immunity. Nat. Immunol. 15, 707–716 (2014).
12. T. J. Wilson, A. Fuchs, M. Colonna, Cutting edge: human FcRl4 and FcRl5 are receptors for IgA and IgG. J. Immunol. 188, 4741–4745 (2012).
13. D. L. Mallery, W. A. McEwan, S. R. Bidgood, G. J. Towers, C. M. Johnson, L. C. James, Antibodies mediate intracellular immunity through tripartite motif-containing 21 (TRIM21). Proc. Natl. Acad. Sci. U.S.A. 107, 19985–19990 (2010).
14. E. Chalayer, B. Gramont, F. Zekre, R. Goguyer-Deschaumes, L. Waeckel, L. Grange, S. Paul, A. W. Chung, M. Killian, Fc receptors gone wrong: a comprehensive review of their roles in autoimmune and inflammatory diseases. Autoimmun. Rev. 21, 103016 (2022).
15. K. G. C. Smith, M. R. Clatworthy, FcγRIIb in autoimmunity and infection: evolutionary and therapeutic implications. Nat. Rev. Immunol. 10, 328–343 (2010).F. galvez- cancino, a. P. Simpson, c. costoya, i. matos, D. Qian, K. S. Peggs, K. litchfield, S. a. Quezada, Fcγ receptors and immunomodulatory antibodies in cancer. *Nat. Rev. Cancer* **24**, 51–71 (2024).
16. F. Galvez-Cancino, A. P. Simpson, C. Costoya, I. Matos, D. Qian, K. S. Peggs, K. Litchfield, S. A. Quezada, Fcγ receptors and immunomodulatory antibodies in cancer. Nat. Rev. Cancer 24, 51–71 (2024).
17. J. I. Robinson, M. Y. M. Yusof, V. Davies, D. Wild, M. Morgan, J. C. Taylor, Y. El- Sherbiny, D. L. Morris, L. Liu, A. C. Rawstron, M. H. Buch, D. Plant, H. J. Cordell, J. D. Isaacs, I. N. Bruce, P. Emery, A. Barton, T. J. Vyse, J. H. Barrett, E. M. Vital, A. W. Morgan, Comprehensive genetic and functional analyses of Fc gamma receptors influence on response to rituximab therapy for autoimmunity. EBioMedicine 86, 104343 (2022).
18. J. S. Verbeek, S. Hirose, H. Nishimura, The complex association of FcγRiib with autoimmune susceptibility. Front. Immunol. 10, 2061 (2019).
19. C.- H. Lee, G. Romain, W. Yan, M. Watanabe, W. Charab, B. Todorova, J. Lee, K. Triplett, M. Donkor, O. I. Lungu, A. Lux, N. Marshall, M. A. Lindorfer, O. R.- L. Goff, B. Balbino, T. H. Kang, H. Tanno, G. Delidakis, C. Alford, R. P. Taylor, F. Nimmerjahn, N.

Published in : Sci. Immunol (2026), vol. 11, n°115
DOI: 10.1126/sciimmunol.ady7328
Status : Postprint (Author's version)

Varadarajan, P. Bruhns, Y. J. Zhang, G. Georgiou, IgG Fc domains that bind C1q but not effector Fcγ receptors delineate the importance of complement-mediated effector functions. Nat. Immunol. 18, 889–898 (2017).

20. G. Delidakis, J. E. Kim, K. George, G. Georgiou, Improving antibody therapeutics by manipulating the Fc Domain: immunological and structural considerations. Annu. Rev. Biomed. Eng. 24, 249–274 (2022).
21. P. Smith, D. J. Dilillo, S. Bournazos, F. Li, J. V. Ravetch, Mouse model recapitulating human Fcγ receptor structural and functional diversity. Proc. Natl. Acad. Sci. U.S.A. 109, 6181–6186 (2012).
22. C. M. Gillis, F. Jönsson, D. A. Mancardi, N. Tu, H. Beutier, N. Van Rooijen, L. E. Macdonald, A. J. Murphy, P. Bruhns, Mechanisms of anaphylaxis in human low-affinity IgG receptor locus knock-in mice. J. Allergy Clin. Immunol. 139, 1253–1265.e14 (2017).
23. E. Casey, S. Bournazos, G. Mo, P. Mondello, K. S. Tan, J. V. Ravetch, D. A. Scheinberg, A new mouse expressing human Fcγ receptors to better predict therapeutic efficacy of human anti-cancer antibodies. Leukemia 32, 547–549 (2018).
24. H. Beutier, B. Hechler, O. Godon, Y. Wang, C. M. Gillis, L. De Chaisemartin, A. Gouel-Chéron, S. Magnenat, L. E. Macdonald, A. J. Murphy, NASA Study Group, S. Chollet-Martin, D. Longrois, C. Gachet, P. Bruhns, F. Jönsson, Platelets expressing IgG receptor FcγRIIa/CD32a determine the severity of experimental anaphylaxis. Sci. Immunol. 3, eaan5997 (2018).
25. A. Lux, M. Seeling, A. Baerenwaldt, B. Lehmann, I. Schwab, R. Repp, N. Meidenbauer, A. Mackensen, A. Hartmann, G. Heidkamp, D. Dudziak, F. Nimmerjahn, A humanized mouse identifies the bone marrow as a niche with low therapeutic IgG activity. Cell Rep. 7, 236–248 (2014).
26. I. Katano, R. Ito, K. Kawai, T. Takahashi, Improved detection of in vivo human NK cell-mediated antibody-dependent cellular cytotoxicity using a novel NOG-FcγR-deficient human IL-15 transgenic mouse. Front. Immunol. 11, 532684 (2020).
27. S. Borghi, S. Bournazos, N. K. Thulin, C. Li, A. Gajewski, R. W. Sherwood, S. Zhang, E. Harris, P. Jagannathan, L.-X. Wang, J. V. Ravetch, T. T. Wang, FcRn, but not FcγRs, drives maternal-fetal transplacental transport of human IgG antibodies. Proc. Natl. Acad. Sci. U.S.A. 117, 12943–12951 (2020).
28. S. Bournazos, D. J. Dilillo, A. J. Goff, P. J. Glass, J. V. Ravetch, Differential requirements for FcγR engagement by protective antibodies against Ebola virus. Proc. Natl. Acad. Sci. U.S.A. 116, 20054–20062 (2019).
29. D. J. Dilillo, G. S. Tan, P. Palese, J. V. Ravetch, Broadly neutralizing hemagglutinin stalk–specific antibodies require FcγR interactions for protection against influenza virus in vivo. Nat. Med. 20, 143–151 (2014).B. Wolf, V. Jeliazkova- mecheva, a. Del Rio- espinola, J. Boisclair, D. Walker, B. cochin De Billy, m. Flaherty, t. Flandre, an afucosylated anti- cD32b monoclonal antibody induced platelet- mediated adverse events in a human Fcγ receptor transgenic mouse model and its potential human translatability. *Toxicol. Sci.* **185**, 89–104 (2022).
30. B. Wolf, V. Jeliazkova-Mècheva, A. Del Rio-Espinola, J. Boisclair, D. Walker, B. Cochin De Billy, M. Flaherty, T. Flandre, An afucosylated anti-CD32b monoclonal antibody induced platelet-mediated adverse events in a human Fcγ receptor transgenic mouse model and its potential human translatability. Toxicol. Sci. 185, 89–104 (2022).
31. J. Lejeune, G. Brachet, H. Watier, Evolutionary story of the low/medium-affinity IgG Fc receptor gene cluster. Front. Immunol. 10, 1297 (2019).
32. C. Kerntke, F. Nimmerjahn, M. Biburger, There is (scientific) strength in numbers: a comprehensive quantitation of Fc gamma receptor numbers on human and murine peripheral blood leukocytes. Front. Immunol. 11, 118 (2020).
33. M. Guilliams, P. Bruhns, Y. Saeys, H. Hammad, B. N. Lambrecht, The function of Fcγ receptors in dendritic cells and macrophages. Nat. Rev. Immunol. 14, 94–108 (2014).
34. J. Van der Heijden, W. B. Breunis, J. Geissler, M. De Boer, T. K. Van den Berg, T. W. Kuijpers, Phenotypic variation in IgG receptors by nonclassical FcgR2c alleles. J. Immunol. 188, 1318–1324 (2012).
35. J. Jorssen, G. V. Hulst, K. Möllers, J. Pujol, G. Petrellis, A. P. Baptista, S. Schetters, F. Baron, J. Caers, B. N. Lambrecht, B. G. Dewals, F. Bureau, C. J. Desmet, Single-cell proteomics and transcriptomics capture eosinophil development and identify the role of IL-5 in their lineage transit amplification. Immunity 57, 1549–1566.e8 (2024).
36. E. Becht, D. Tolstrup, C.-A. Dutertre, P. A. Morawski, D. J. Campbell, F. Ginhoux, E. W. Newell, R. Gottardo, M. B. Headley, High-throughput single-cell quantification of hundreds of proteins using conventional flow cytometry and machine learning. Sci. Adv. 7, eabg0505 (2021).
37. I. Kwok, E. Becht, Y. Xia, M. Ng, Y. C. Teh, L. Tan, M. Evrard, J. L. Y. Li, H. T. N. Tran, Y. Tan, D. Liu, A. Mishra, K. H. Liong, K. Leong, Y. Zhang, A. Olsson, C. K. Mantri, P. Shyamsunder, Z. Liu, C. Piot, C.-A. Dutertre, H. Cheng, S. Bari, N. Ang, S. K. Biswas, H. P. Koeffler, H. L. Tey, Larbi, I.-H. Su, B. Lee, A. St. John, J. K. Y. Chan, W. Y. K. Hwang, J. Chen, N. Salomonis, S. Z. Chong, H. L. Grimes, B. Liu, A. Hidalgo, E. W. Newell, T. Cheng, F. Ginhoux, L. G. Ng, Combinatorial single-cell analyses of granulocyte-monocyte progenitor heterogeneity reveals an early uni-potent neutrophil progenitor. Immunity 53, 303–318.e5 (2020).
38. A. J. Kwok, A. Allcock, R. C. Ferreira, E. Cano-Gomez, M. Smee, K. L. Burnham, Y.-X. Zurke, S. McKechnie, A. J. Mentzer, C. Monaco, I. A. Udalova, C. J. Hinds, J. A. Todd, E. E. Davenport, J. C. Knight, Neutrophils and emergency granulopoiesis drive immune suppression and an extreme response endotype during sepsis. Nat. Immunol. 24, 767–779 (2023).
39. Tabula Sapiens Consortium, The Tabula Sapiens: a multiple-organ, single-cell transcriptomic atlas of humans. Science 376, eabl4896 (2022).

Published in : Sci. Immunol (2026), vol. 11, n°115
DOI: 10.1126/sciimmunol.ady7328
Status : Postprint (Author's version)

40. S. Bhandari, A. K. Larsen, P. McCourt, B. Smedsrød, K. K. Sørensen, The scavenger function of liver sinusoidal endothelial cells in health and disease. Front. Physiol. 12, 757469 (2021).
41. T. Takai, M. Li, D. Sylvestre, R. Clynes, J. V. Ravetch, FcR γ chain deletion results in pleiotropic effector cell defects. Cell 76, 519–529 (1994).
42. A.-C. Villani, R. Satija, G. Reynolds, S. Sarkizova, K. Shekhar, J. Fletcher, M. Griesbeck, Butler, S. Zheng, S. Lazo, L. Jardine, D. Dixon, E. Stephenson, E. Nilsson, I. Grundberg, D. McDonald, A. Filby, W. Li, P. L. De Jager, O. Rozenblatt-Rosen, A. A. Lane, M. Haniffa, A. Regev, N. Hacohen, Single-cell RNA-seq reveals new types of human blood dendritic cells, monocytes, and progenitors. Science 356, eaah4573 (2017).
43. P. Badia-i-mompel, J. Vélez Santiago, J. Braunger, C. Geiss, D. Dimitrov, S. Müller-Dott, P. Taus, A. Dugourd, C. H. Holland, R. O. Ramirez Flores, J. Saez-Rodriguez, DecoupleR: ensemble of computational methods to infer biological activities from omics data. Bioinform. Adv. 2, vbac016 (2022).
44. P. M. Guyre, P. M. Morganelli, R. Miller, Recombinant immune interferon increases immunoglobulin G Fc receptors on cultured human mononuclear phagocytes. J. Clin. Invest. 72, 393–397 (1983).
45. L. Pricop, P. Redecha, J.-L. Teillaud, J. Frey, W. H. Fridman, C. Sautès-Fridman, J. E. Salmon, Differential modulation of stimulatory and inhibitory Fcγ receptors on human monocytes by Th1 and Th2 cytokines. J. Immunol. 166, 531–537 (2001).
46. C. Bosteels, K. Neyt, M. Vanheerswynghels, M. J. Van Helden, D. Sichien, N. Debeuf, S. De Prijck, V. Bosteels, N. Vandamme, L. Martens, Y. Saeys, E. Louagie, M. Lesage, D. L. Williams, S. C. Tang, J. U. Mayer, F. Ronchese, C. L. Scott, H. Hammad, M. Guilliams, B. N. Lambrecht, Inflammatory type 2 cDCs acquire features of cDC1s and macrophages to orchestrate immunity to respiratory virus infection. Immunity 52, 1039–1056.e9 (2020).
47. A. M. Brandsma, S. L. Schwartz, M. J. Wester, C. C. Valley, G. L. A. Blezer, G. Vidarsson, K. A. Lidke, T. ten Broeke, D. S. Lidke, J. H. W. Leusen, Mechanisms of inside-out signaling of the high-affinity IgG receptor FcγRI. Sci. Signal. 11, eaaq0891 (2018).
48. O. Wood, A. T. Braithwaite, J. Fisher, L. Liu, L. Murray, C. Paluch, M. A. Jackson-Wood, Intra- and intercellular immune responses across diverse in vitro stimuli and inflammatory disease. bioRxiv 661918 [Preprint] (2025). https://doi.org/10.1101/2025.06.27.661918.
49. P. Jiang, Y. Zhang, B. Ru, Y. Yang, T. Vu, R. Paul, A. Mirza, G. Altan-Bonnet, L. Liu, E. Ruppin, L. Wakefield, K. W. Wucherpfennig, Systematic investigation of cytokine signaling activity at the tissue and single-cell levels. Nat. Methods 18, 1181–1191 (2021).
50. R. Browaeys, W. Saelens, Y. Saeys, Nichenet: modeling intercellular communication by linking ligands to target genes. Nat. Methods 17, 159–162 (2020).
51. R. Browaeys, J. Gilis, C. Sang-Aram, P. D. Bleser, L. Hoste, S. Tavernier, D. Lambrechts, R. Seurinck, Y. Saeys, Multinichenet: a flexible framework for differential cell-cell communication analysis from multi-sample multi-condition single-cell transcriptomics data. bioRxiv 544751 [Preprint] (2023). https://doi.org/10.1101/2023.06.13.544751.
52. Bournazos, T. T. Wang, J. V. Ravetch, The role and function of Fcγ receptors on myeloid cells. Microbiol. Spectr. 4, 10.1128/microbiolspec.mchD-0045-2016 (2016).
53. C. Bravo-González-Blas, S. De Winter, G. Hulselmans, N. Hecker, I. Matetovici, V. Christiaens, S. Poovathingal, J. Wouters, S. Aibar, S. Aerts, Scenic+: Single-cell multiomic inference of enhancers and gene regulatory networks. Nat. Methods 20, 1355–1367 (2023).
54. ENCODE Project Consortium, An integrated encyclopedia of DNA elements in the human genome. Nature 489, 57–74 (2012).
55. K. L. Lewis, M. L. Caton, M. Bogunovic, M. Greter, L. T. Grajkowska, D. Ng, A. Klinakis, I. F. Charo, S. Jung, J. L. Gommerman, I. I. Ivanov, K. Liu, M. Merad, B. Reizis, Notch2 receptor signaling controls functional differentiation of dendritic cells in the spleen and intestine. Immunity 35, 780–791 (2011).
56. C. Minutti, C. Piot, M. Pereira da Costa, P. Chakravarty, N. Rogers, H. Huerga Encabo, Cardoso, J. Loong, G. Bessou, C. Mionnet, J. Langhorne, D. Bonnet, M. Dalod, E. Tomasello, C. Reis e Sousa, Distinct ontogenetic lineages dictate cDC2 heterogeneity. Nat. Immunol. 25, 448–461 (2024).
57. C. C. Brown, H. Gudjonson, Y. Pritykin, D. Deep, V.-P. Lavallée, A. Mendoza, R. Fromme, L. Mazutis, C. Ariyan, C. Leslie, D. Pe'er, A. Y. Rudensky, Transcriptional basis of mouse and human dendritic cell heterogeneity. Cell 179, 846–863.e24 (2019).
58. S. A. Mousavi, M. Sporstøl, C. Fladeby, R. Kjeken, N. Barois, T. Berg, Receptor-mediated endocytosis of immune complexes in rat liver sinusoidal endothelial cells is mediated by FcγRiib2. Hepatology 46, 871–884 (2007).
59. Z. Liu, H. Wang, Z. Li, R. J. Dress, Y. Zhu, S. Zhang, D. De Feo, W. T. Kong, P. Cai, A. Shin, C. Piot, J. Yu, Y. Gu, M. Zhang, C. Gao, L. Chen, H. Wang, M. Vétillard, P. Guermonprez, I. Kwok, L. G. Ng, S. Chakarov, A. Schlitzer, B. Becher, C.-A. Dutertre, B. Su, F. Ginhoux, Dendritic cell type 3 arises from LY6C+ monocyte-dendritic cell progenitors. Immunity 56, 1761–1777.e6 (2023).
60. M. Pyzik, T. Rath, T. T. Kuo, S. Win, K. Baker, J. J. Hubbard, R. Grenha, A. Gandhi, T. D. Krämer, A. R. Mezo, Z. S. Taylor, K. McDonnell, V. Nienaber, J. T. Andersen, Mizoguchi, L. Blumberg, S. Purohit, S. D. Jones, G. Christianson, W. I. Lencer, I. Sandlie, N. Kaplowitz, D. C. Roopenian, R. S. Blumberg, Hepatic FcRn regulates albumin homeostasis and susceptibility to liver injury. Proc. Natl. Acad. Sci. U.S.A. 114, e2862–e2871 (2017).

Published in : Sci. Immunol (2026), vol. 11, n°115
DOI: 10.1126/sciimmunol.ady7328
Status : Postprint (Author's version)

61. H. P. Montoyo, C. Vaccaro, M. Hafner, R. J. Ober, W. Mueller, E. S. Ward, Conditional deletion of the MHC class I-related receptor FcRn reveals the sites of IgG homeostasis in mice. Proc. Natl. Acad. Sci. U.S.A. 106, 2788–2793 (2009).
62. Tabula Muris Consortium, Overall coordination, logistical coordination, organ collection and processing, library preparation and sequencing, computational data analysis, cell type annotation, writing group, supplemental text writing group, principal investigators, single-cell transcriptomics of 20 mouse organs creates a Tabula Muris. Nature 562, 367–372 (2018).
63. A. Cui, T. Huang, S. Li, A. Ma, J. L. Pérez, C. Sander, D. B. Keskin, C. J. Wu, E. Fraenkel, N. Hacohen, Dictionary of immune responses to cytokines at single-cell resolution. Nature 625, 377–384 (2024).
64. E. Vivier, E. Tomasello, M. Baratin, T. Walzer, S. Ugolini, Functions of natural killer cells. Nat. Immunol. 9, 503–510 (2008).
65. A. Baysoy, K. Seddu, T. Salloum, C. A. Dawson, J. J. Lee, L. Yang, S. Gal- Oz, H. Ner-Gaon, J. Tellier, A. Millan, A. Sasse, B. Brown, L. L. Lanier, T. Shay, S. Nutt, D. Dwyer, C. Benoist, Immunological Genome Project Consortium, The interweaved signatures of common-gamma-chain cytokines across immunologic lineages. J. Exp. Med. 220, e20222052 (2023).
66. F. Hammal, P. De Langen, A. Bergon, F. Lopez, B. Ballester, Remap 2022: a database of human, mouse, Drosophila and Arabidopsis regulatory regions from an integrative analysis of DNA-binding sequencing experiments. Nucleic Acids Res. 50, D316–D325 (2022).
67. C.-H. Chen, R. Zheng, C. Tokheim, X. Dong, J. Fan, C. Wan, Q. Tang, M. Brown, J. S. Liu, C. A. Meyer, X. S. Liu, Determinants of transcription factor regulatory range. Nat. Commun. 11, 2472 (2020).
68. F. R. Brennan, J. Cavagnaro, K. McKeever, P. C. Ryan, M. M. Schutten, J. Vahle, G. F. Weinbauer, E. Marrer-Berger, L. E. Black, Safety testing of monoclonal antibodies in non-human primates: case studies highlighting their impact on human risk assessment. MAbs 10, 1–17 (2017).
69. J. Elhmouzi-Younes, J.-L. Palgen, N. Tchitchek, S. Delandre, I. Namet, C. L. Bodinham, K. Pizzoferro, D. J. M. Lewis, R. Le Grand, A. Cosma, A.-S. Beignon, In-depth comparative phenotyping of blood innate myeloid leukocytes from healthy humans and macaques using mass cytometry. Cytometry A 91, 969–982 (2017).
70. L. Han, X. Wei, C. Liu, G. Volpe, Z. Zhuang, X. Zou, Z. Wang, T. Pan, Y. Yuan, X. Zhang, P. Fan, P. Guo, Y. Lai, Y. Lei, X. Liu, F. Yu, S. Shangguan, G. Lai, Q. Deng, Y. Liu, L. Wu, Q. Shi, H. Yu, Y. Huang, M. Cheng, J. Xu, Y. Liu, M. Wang, C. Wang, Y. Zhang, D. Xie, Y. Yang, Y. Yu, H. Zheng, Y. Wei, F. Huang, J. Lei, W. Huang, Z. Zhu, H. Lu, B. Wang, X. Wei, F. Chen, T. Yang, W. Du, J. Chen, S. Xu, Jan, C. Ward, Z. Wang, Z. Pei, C.-W. Wong, X. Liu, H. Zhang, M. Liu, B. Qin, A. Schambach, J. Isern, L. Feng, Y. Liu, X. Guo, Z. Liu, Q. Sun, P. H. Maxwell, N. Barker, P. Muñoz-Cánoves, Y. Gu, J. Mulder, M. Uhlen, T. Tan, S. Liu, H. Yang, J. Wang, Y. Hou, X. Xu, M. A. Esteban, L. Liu, Cell transcriptomic atlas of the non-human primate Macaca fascicularis. Nature 604, 723–731 (2022).
71. D. Viuff, F. Antunes, L. Evans, J. Cameron, H. Dyrnesli, B. Thue Ravn, M. Stougaard, K. Thiam, B. Andersen, S. Kjærulff, K. A. Howard, Generation of a double transgenic humanized neonatal Fc receptor (FcRn)/albumin mouse to study the pharmacokinetics of albumin-linked drugs. J. Control. Release 223, 22–30 (2016).
72. R. J. Ober, C. G. Radu, V. Ghetie, E. S. Ward, Differences in promiscuity for antibody–FcRn interactions across species: implications for therapeutic antibodies. Int. Immunol. 13, 1551–1559 (2001).
73. Z. Xiang, A. J. Cutler, R. J. Brownlie, K. Fairfax, K. E. Lawlor, E. Severinson, E. U. Walker, R. A. Manz, D. M. Tarlinton, K. G. C. Smith, FcγRiib controls bone marrow plasma cell persistence and apoptosis. Nat. Immunol. 8, 419–429 (2007).
74. T. Takai, M. Ono, M. Hikida, H. Ohmori, J. V. Ravetch, Augmented humoral and anaphylactic responses in FcγRII- deficient mice. Nature 379, 346–349 (1996).
75. M. Guilliams, J. Bonnardel, B. Haest, B. Vanderborght, C. Wagner, A. Remmerie, A. Bujko, L. Martens, T. Thoné, R. Browaeys, F. F. De Ponti, B. Vanneste, C. Zwicker, F. R. Svedberg, T. Vanhalewyn, A. Gonçalves, S. Lippens, B. Devriendt, E. Cox, G. Ferrero, V. Wittamer, Willaert, S. J. F. Kaptein, J. Neyts, K. Dallmeier, P. Geldhof, S. Casaert, B. Deplancke, P. Ten Dijke, A. Hoorens, A. Vanlander, F. Berrevoet, Y. Van Nieuwenhove, Y. Saeys, W. Saelens, H. Van Vlierberghe, L. Devisscher, C. L. Scott, Spatial proteogenomics reveals distinct and evolutionarily conserved hepatic macrophage niches. Cell 185, 379–396.e38 (2022).
76. Y. N. Abdiche, Y. A. Yeung, J. Chaparro-R Igger, I. Barman, P. Strop, S. M. Chin, A. Pham, G. Bolton, D. McDonough, K. Lindquist, J. Pons, A. Rajpal, The neonatal Fc receptor (FcRn) binds independently to both sites of the IgG homodimer with identical affinity. MAbs 7, 331–343 (2015).
77. D. Corti, J. Voss, S. J. Gamblin, G. Codoni, A. Macagno, D. Jarrossay, S. G. Vachieri, D. Pinna, Minola, F. Vanzetta, C. Silacci, B. M. Fernandez-Rodriguez, G. Agatic, S. Bianchi, I. Giacchetto-Sasselli, L. Calder, F. Sallusto, P. Collins, L. F. Haire, N. Temperton, J. P. M. Langedijk, J. J. Skehel, A. Lanzavecchia, A neutralizing antibody selected from plasma cells that binds to group 1 and group 2 influenza A hemagglutinins. Science 333, 850–856 (2011).
78. N. L. Kallewaard, D. Corti, P. J. Collins, U. Neu, J. M. Mcauliffe, E. Benjamin, L. Wachter-Rosati, F. J. Palmer-Hill, A. Q. Yuan, P. A. Walker, M. K. Vorlaender, S. Bianchi, B. Guarino, A. De Marco, F. Vanzetta, G. Agatic, M. Flaherty, D. Pinna, B. Fernandez-Rodriguez, A. Fruehwirth, C. Silacci, R. W. Ogrodowicz, S. R. Martin, F. Sallusto, J. A. Suzich, A. Lanzavecchia, Q. Zhu, S. J. Gamblin, J. J. Skehel, Structure and function analysis of an antibody recognizing all influenza A subtypes. Cell 166, 596–608 (2016).
79. R. Liu, R. J. Oldham, E. Teal, S. A. Beers, M. S. Cragg, Fc-engineering for modulated effector functions—improving antibodies for cancer treatment. Antibodies 9, 64 (2020).

Published in : Sci. Immunol (2026), vol. 11, n°115
DOI: 10.1126/sciimmunol.ady7328
Status : Postprint (Author's version)

80. J. O. Richards, S. Karki, G. A. Lazar, H. Chen, W. Dang, J. R. Desjarlais, Optimization of antibody binding to FcγRiia enhances macrophage phagocytosis of tumor cells. Mol. Cancer Ther. 7, 2517–2527 (2008).
81. P. Weitzenfeld, S. Bournazos, J. V. Ravetch, Antibodies targeting sialyl Lewis A mediate tumor clearance through distinct effector pathways. J. Clin. Invest. 129, 3952–3962 (2019).
82. S. Bournazos, D. Corti, H. W. Virgin, J. V. Ravetch, Fc-optimized antibodies elicit CD8 immunity to viral respiratory infection. Nature 588, 485–490 (2020).
83. A. Ahuja, J. Shupe, R. Dunn, M. Kashgarian, M. R. Kehry, M. J. Shlomchik, Depletion of B cells in murine lupus: efficacy and resistance. J. Immunol. 179, 3351–3361 (2007).
84. A. R. Temming, A. E. H. Bentlage, S. W. De Taeye, G. P. Bosman, S. N. Lissenberg-Thunnissen, N. I. L. Derksen, G. Brasser, J. Y. Mok, W. J. E. Van Esch, H. L. Howie, J. C. Zimring, G. Vidarsson, Cross-reactivity of mouse IgG subclasses to human Fc gamma receptors: antibody deglycosylation only eliminates IgG2b binding. Mol. Immunol. 127, 79–86 (2020).
85. S. D. Liu, J. B. Lowe, Implications of understanding the signaling, cellular, and cytotoxic mechanisms afforded by afucosylated antibodies. Onco Targets Ther. 4, e1009288 (2015).
86. L. Gauthier, A. Morel, N. Anceriz, B. Rossi, A. Blanchard-Alvarez, G. Grondin, S. Trichard, C. Cesari, M. Sapet, F. Bosco, H. Rispaud-Blanc, F. Guillot, S. Cornen, A. Roussel, B. Amigues, G. Habif, F. Caraguel, S. Arrufat, R. Remark, F. Romagné, Y. Morel, E. Narni-Mancinelli, E. Vivier, Multifunctional natural killer cell engagers targeting NKp46 trigger protective tumor immunity. Cell 177, 1701–1713.e16 (2019).
87. O. Demaria, L. Gauthier, M. Vetizou, A. Blanchard-Alvarez, C. Vagne, G. Habif, L. Batista, W. Baron, N. Belaïd, M. Girard-Madoux, C. Cesari, M. Caratini, F. Bosco, O. Benac, J. Lopez, Fenis, J. Galluso, S. Trichard, B. Carrette, F. Carrette, A. Maguer, S. Jaubert, A. Sansaloni, R. Letay-Drouet, C. Kosthowa, N. Lovera, A. Dujardin, F. Chanuc, M. Le Van, S. Bokobza, N. Jarmuzynski, C. Fos, N. Gourdin, R. Remark, E. Lechevallier, N. Fakhry, S. Salas, J.-L. Deville, R. Le Grand, C. Bonnafous, L. Vollmy, A. Represa, S. Carpentier, B. Rossi, A. Morel, S. Cornen, I. Perrot, Y. Morel, E. Vivier, Antitumor immunity induced by antibody-based natural killer cell engager therapeutics armed with non-alpha IL-2 variant. Cell Rep. Med. 3, 100783 (2022).
88. C. Madesan, D. Matesoi, C. Radu, V. Ghetie, E. S. Ward, Delineation of the amino acid residues involved in transcytosis and catabolism of mouse IgG1. J. Immunol. 158, 2211–2217 (1997).
89. O. A. Aguilar, L.-K. Fong, K. Ishiyama, W. F. Degrado, L. L. Lanier, The CD3ζ adaptor structure determines functional differences between human and mouse CD16 Fc receptor signaling. J. Exp. Med. 219, e20220022 (2022).
90. Z. B. Bjornson-Hooper, G. K. Fragiadakis, M. H. Spitzer, H. Chen, D. Madhireddy, K. Hu, K. Lundsten, D. R. McIlwain, G. P. Nolan, A comprehensive atlas of immunological differences between humans, mice, and non-human primates. Front. Immunol. 13, 867015 (2022).
91. K. M. Semple, C. M. Gonzaléz, M. Zarr, J. R. Austin, V. Patel, K. E. Howard, Evaluation of the ability of immune humanized mice to demonstrate CD20-specific cytotoxicity induced by Ofatumumab. Clin. Transl. Sci. 12, 283–290 (2019).
92. A. Gupta, P. Smith, S. Bournazos, J. V. Ravetch, A novel mouse strain optimized for chronic human antibody administration. Proc. Natl. Acad. Sci. U.S.A. 119, e2123002119 (2022).
93. C.-H. Lee, T. H. Kang, O. Godon, M. Watanabe, G. Delidakis, C. M. Gillis, D. Sterlin, D. Hardy, M. Congé, L. E. Macdonald, A. J. Murphy, N. Tu, J. Lee, J. R. McDaniel, E. Makowski, P. M. Tessier, A. S. Meyer, P. Bruhns, G. Georgiou, An engineered human Fc domain that behaves like a pH-toggle switch for ultra-long circulation persistence. Nat. Commun. 10, 5031 (2019).
94. M. Guilliams, C.-A. Dutertre, C. L. Scott, N. McGovern, D. Sichien, S. Chakarov, S. Van Gassen, J. Chen, M. Poidinger, S. De Prijck, S. J. Tavernier, I. Low, S. E. Irac, C. N. Mattar, H. R. Sumatoh, G. H. L. Low, T. J. K. Chung, D. K. H. Chan, K. K. Tan, T. L. K. Hon, E. Fossum, B. Bogen, M. Choolani, J. K. Y. Chan, A. Larbi, H. Luche, S. Henri, Y. Saeys, E. W. Newell, B. N. Lambrecht, B. Malissen, F. Ginhoux, Unsupervised high-dimensional analysis aligns dendritic cells across tissues and species. Immunity 45, 669–684 (2016).
95. G. J. Christianson, V. Z. Sun, S. Akilesh, E. Pesavento, G. Proetzel, D. C. Roopenian, Monoclonal antibodies directed against human FcRn and their applications. MAbs 4, 208–216 (2012).
96. M. W. Kristensen, S. Kejlberg-Jensen, A. S. Sørensen, T. Vorup-Jensen, T. W. Kragstrup, M. Hokland, M. N. Andersen, Behold cytometrists: one block is not enough! Cyanine-tandems bind non-specifically to human monocytes. Cytometry A 99, 265–268 (2021).
97. V. Hox, A. Desai, G. Bandara, A. Gilfillan, D. D. Metcalfe, A. Olivera, Estrogen increases the severity of anaphylaxis in female mice through enhanced endothelial nitric oxide synthase expression and nitric oxide production. J. Allergy Clin. Immunol. 135, 729–36.e5 (2015).
98. J. Bonnardel, W. T'Jonck, D. Gaublomme, R. Browaeys, C. L. Scott, L. Martens, B. Vanneste, S. De Prijck, S. A. Nedospasov, A. Kremer, E. Van Hamme, P. Borghgraef, W. Toussaint, P. De Bleser, I. Mannaerts, A. Beschin, L. A. Van Grunsven, B. N. Lambrecht, T. Taghon, S. Lippens, D. Elewaut, Y. Saeys, M. Guilliams, Stellate cells, hepatocytes, and endothelial cells imprint the Kupffer cell identity on monocytes colonizing the liver macrophage niche. Immunity 51, 638–654.e9 (2019).
99. W. Saelens, R. Cannoodt, H. Todorov, Y. Saeys, A comparison of single-cell trajectory inference methods. Nat. Biotechnol. 37, 547–554 (2019).

Published in : Sci. Immunol (2026), vol. 11, n°115
DOI: 10.1126/sciimmunol.ady7328
Status : Postprint (Author's version)

100. C. L. Sokol, N.-Q. Chu, S. Yu, S. A. Nish, T. M. Laufer, R. Medzhitov, Basophils function as antigen-presenting cells for an allergen-induced T helper type 2 response. Nat. Immunol. 10, 713–720 (2009).
101. I. Van de Walle, G. De Smet, M. Gärtner, M. De Smedt, E. Waegemans, B. Vandekerckhove, G. Leclercq, J. Plum, J. C. Aster, I. D. Bernstein, C. J. Guidos, B. Kyewski, T. Taghon, Jagged2 acts as a Delta-like notch ligand during early hematopoietic cell fate decisions. Blood 117, 4449–4459 (2011).
102. J. Xue, B. S. Chambers, S. E. Hensley, C. B. López, Propagation and characterization of influenza virus stocks that lack high levels of defective viral genomes and hemagglutinin mutations. Front. Microbiol. 7, 326 (2016).
103. M. I. Love, W. Huber, S. Anders, Moderated estimation of fold change and dispersion for RNA-seq data with DESeq2. Genome Biol. 15, 550 (2014).
104. C. A. Sloan, E. T. Chan, J. M. Davidson, V. S. Malladi, J. S. Strattan, B. C. Hitz, I. Gabdank, K. Narayanan, M. Ho, B. T. Lee, L. D. Rowe, T. R. Dreszer, G. Roe, N. R. Podduturi, F. Tanaka, E. L. Hong, J. M. Cherry, ENCODE data at the ENCODE portal. Nucleic Acids Res. 44, D726–D732 (2016).
105. S. G. Landt, G. K. Marinov, A. Kundaje, P. Kheradpour, F. Pauli, S. Batzoglou, B. E. Bernstein, P. Bickel, J. B. Brown, P. Cayting, Y. Chen, G. DeSalvo, C. Epstein, K. I. Fisher-Aylor, G. Euskirchen, M. Gerstein, J. Gertz, A. J. Hartemink, M. M. Hoffman, V. R. Iyer, Y. L. Jung, S. Karmakar, M. Kellis, P. V. Kharchenko, Q. Li, T. Liu, X. S. Liu, L. Ma, A. Milosavljevic, R. M. Myers, P. J. Park, M. J. Pazin, M. D. Perry, D. Raha, T. E. Reddy, J. Rozowsky, N. Shoresh, Sidow, M. Slattery, J. A. Stamatoyannopoulos, M. Y. Tolstorukov, K. P. White, S. Xi, P. J. Farnham, J. D. Lieb, B. J. Wold, M. Snyder, ChIP-seq guidelines and practices of the ENCODE and modENCODE consortia. Genome Res. 22, 1813–1831 (2012).
106. C.-H. Gao, G. Yu, P. Cai, ggVennDiagram: an intuitive, easy-to-use, and highly customizable R package to generate Venn diagram. Front. Genet. 12, 706907 (2021).).

Acknowledgments: We thank the ViB core Facilities (Single cell, Flow, Protein, and Bioimaging core), ViB tech Watch (irina matetovici and toon Swings), all iRc animal caretakers, and the lambrecht and the Janssens labs for experimental support. We thank S. Ward (university of Southampton) for the fluorescent labeling of Synt002. We are grateful to h. Baggali for critically reviewing the manuscript. **Funding:** this research was supported by a Vlaio research grant Bc.2020.3084 (B.n.l., argenx); eRc consolidator grant DcRiDDle- 819314 (S.J.); and Research Foundation- Flanders, Belgium (FWo) grant 1244321n and FWo grant g0a7422n (S. Vanhee). **Author contributions:** conceptualization: K.F.a.V.D., D.S., K.V.d.B., a.m., e.V., F.S., K.t., S. Voet, B.B., and B.n.l. methodology: S.V.g., J.J., S.D.W., P.D.B., c.D.n., R.B., K.Q., J.D., t.h., S. Vanhee, and a.P.B. investigation: K.F.a.V.D., D.S., K.V.d.B., J.V.m., e.D.l., c.W., Q.c., a.B.Z., m.a.S., S.S., V.B., m.V., S.D.P., a.P.B., m.J.S., B.V.D.e., i.R., P.i.P., S.a., and R.c. Supervision: c.l.S., S.a., S.J., y.S., a.J.K., F.B., D.c., n.V., c.D., D.e., h.h., a.m., e.V., F.S., K.t., S. Voet, B.B., and B.n.l. Funding: S. Voet and B.n.l. original draft: K.F.a.V.D. Reviewing and editing of the manuscript: all authors. **Competing interests:** D.S., B.V.D.e., i.R., S.V., and B.B. are full- time employees of argenx BV. the employees of argenx set forth in this manuscript may be described or claimed in planned patent filings, pending patent applications, and/or granted patents. one or more of the authors may presently, or in the future, be named as inventors in one or more of those legal instruments. a.B. is an employee of tribune therapeutics and holds stock options. P.i.P., F.S., and K.t. are employees and hold stock options of genOway. S.a., R.c., a.m., and e.V. are employees of innate Pharma. c.W., Q.c., a.B.Z., m.a.S., F.B., a.J.K., and D.c. are or were employees of Vir Biotechnology and may hold shares in Vir Biotechnology. all remaining authors declare that they have no competing interests. **Data, code, and materials availability:** all data are available in the main text, the Supplementary materials, and the deposited or publicly available datasets. tabulated data underlying Figs. 4 and 6 are provided in data file S15. the raw sequencing data and Seurat objects generated in this publication have been deposited in ncBi's gene expression omnibus and are accessible through geo under accession number gSe261975. the mouse spleen single- cell dataset presented in this manuscript can be accessed via our online tool: www.single- cell.be/splenic_immune_cell_ compartment. the analysis scripts used for analyzing the splenic immune scRna- seq, public single- cell and bulk Rna- seq, prior knowledge models, flow cytometry visualization, and gene regulatory potential scoring have been deposited in a github repository that is publicly accessible at https://github.com/blambrechtlab/fcgammareceptors and https://github.com/ kfvdamme/Fc- gamma- receptors. an archive of the github repository can be downloaded from Zenodo: https://zenodo.org/records/17041603. the humanized mice are commercially available through genoway (www.genoway.com/product/catalog/fcgr and www.genoway. com/product/catalog/geno- hfcgr- hfcrn). anti- cD20 antibody–based nK cell engager therapeutics are available from innate Pharma under a material transfer agreement with the company. all other materials (or code) used or generated in this study are commercially available or will be supplied upon reasonable request.